

REVIEW ARTICLE

Geometric Evolution Laws for Thin Crystalline Films: Modeling and Numerics

Bo Li¹, John Lowengrub², Andreas Rätz³ and Axel Voigt^{2,3,4,*}

¹ *Department of Mathematics and Center for Theoretical Biological Physics,
University of California at San Diego, La Jolla, CA 92093-0112, USA.*

² *Department of Mathematics, University of California at Irvine, Irvine,
CA 92697-3875, USA.*

³ *Institut für Wissenschaftliches Rechnen, Technische Universität Dresden, 01062
Dresden, Germany.*

⁴ *Department of Physics, Technical University of Helsinki, 02015 Espoo, Finland.*

Received 7 October 2008; Accepted (in revised version) 22 January 2009

Available online 6 February 2009

Abstract. Geometrical evolution laws are widely used in continuum modeling of surface and interface motion in materials science. In this article, we first give a brief review of various kinds of geometrical evolution laws and their variational derivations, with an emphasis on strong anisotropy. We then survey some of the finite element based numerical methods for simulating the motion of interfaces focusing on the field of thin film growth. We discuss the finite element method applied to front-tracking, phase-field and level-set methods. We describe various applications of these geometrical evolution laws to materials science problems, and in particular, the growth and morphologies of thin crystalline films.

PACS: 05.70.Np, 02.60.Cb, 02.70.Bf, 02.70.Dh, 81.15.Aa

Key words: Interface problems, geometric evolution laws, anisotropy, kinetics, front tracking, level-set, phase-field, chemical vapor deposition, molecular beam epitaxy, liquid phase epitaxy, electrodeposition.

Contents

1	Introduction	434
2	Anisotropic evolution laws in materials science	436

*Corresponding author. *Email addresses:* bli@math.ucsd.edu (B. Li), lowengrb@math.uci.edu (J. Lowengrub), andreas.raetz@tu-dresden.de (A. Rätz), axel.voigt@tu-dresden.de (A. Voigt)

3	Numerical approaches	443
4	Applications to crystalline thin films	466
5	Conclusions	475

1 Introduction

The engineering of materials with advanced properties requires the innovative design and precise control of material microstructures at micron and nanometer scales. These microstructural patterns are often characterized by interfaces—individual interfaces or interface networks—which evolve during material treatment and manufacture [12, 57, 123]. Here interfaces are understood in a broad sense: an interface can be a geometrical surface that has no thickness—a sharp interface; it can also mean a diffuse interface that can have certain thickness, e.g., of a few atomic diameters. Common examples of material interfaces include solid-liquid boundaries in solidification where a typical example is the ice-water interface near the freezing temperature of water, solid-gas boundaries such as crystal surfaces, phase interfaces in solid-solid phase transformations such as precipitate and martensite interfaces, and domain boundaries that separate different parts of material such as grain boundaries in polycrystals and domain walls in ferromagnetic materials. Compared with those of bulk phases, the properties of material interfaces can be more and more important as the length scales in devices become smaller and smaller. Evolving interfaces therefore are a key ingredient in many problems in materials science, particularly in nanoscale science and technology, and hence require more detailed consideration than in traditional material modeling.

A class of interface problems that we are particularly interested in arise from the modeling of self-organized nanoscale structures on thin solid films. Such structures consist of a large number of spatially ordered atomic objects such as quantum dots and nanowires with narrow size distributions. They possess remarkable optical, electrical, and mechanical properties that have emerging applications in many technological areas. The nucleation, coarsening, and stabilization of such patterned nanostructures are determined largely by the process of growing thin solid films in which surface energies, surface kinetics, bulk strains, and applied fields can play important roles. Accurate and efficient modeling and simulation of growth processes and surface morphologies of thin films are therefore crucial in understanding fundamental constituent mechanisms and further helping the fabrication of self-organized nanostructures on thin films.

There are mainly two kinds of continuum models of material interfaces: sharp interface models and diffuse-interface/phase-field models. In the former, individual interfaces are tracked during their relaxation and evolution. Evolving sharp interfaces are often described by motions of geometrical surfaces that have no thickness and that move with prescribed velocities that typically depend on the interface shape. Two of such geometrical motions that have important applications in material modeling are the motion by mean curvature and that by the surface Laplacian of mean curvature. In phase-field

models, interfaces are characterized by order parameters that have nearly constant values in different regions with a very thin and smooth transition region that represents the interfaces. These order parameters are solutions to field equations and many physical quantities can be expressed through such parameters. For instance, solutions to a heat equation lead to the heat flux which, together with local geometry, determines the motion of a solid-liquid interface in solidification.

Partial differential equations that describe interface motion are often complicated and can only be solved analytically in very special cases. Numerical simulations are therefore important. But it is clear that solving interface problems numerically can be very difficult because of the strong nonlinearity, anisotropy, coupling of geometry and evolutionary differential equations, and multiple spatial and temporal scales from physical models and numerical discretization. Our mathematical understanding of interface motion is far from being complete and satisfactory. This makes the design and improvement of numerical algorithms even more challenging. Over the last few decades, many basic numerical methods have been developed. In recent years, there has been significant progress in the development of innovative numerical methods for simulating interface motion in materials modeling. In both the sharp and phase-field contexts, accurate, efficient, and robust numerical methods have been developed for high-order partial differential equations that characterize evolving surfaces. New methods that also account for coupling with bulk processes have also been developed. In addition, the connections between sharp interface and phase-field models have been further elucidated.

In this article, we first review various kinds of geometrical evolution laws and briefly describe their derivation using variational methods. The basic models are the motion by mean curvature and by the Laplacian of mean curvature. We shall describe how these models can be generalized to include strong surface anisotropy in the surface free energy as well as higher order regularization terms. In some cases, the resulting geometric evolution law is a highly nonlinear 6th order partial differential equation. We then survey some of the recently developed numerical methods for tracking the motion of surfaces and discuss techniques for coupling the evolution with field equations in the bulk with a focus on thin film growth. A key aspect thereby is the combination of various mass transport phenomena and strong anisotropies. Although there have been significant advances in finite difference methods and in discrete approaches (e.g. Monte-Carlo methods) applied to models of interface evolution, we limit the scope of this article to finite element methods. We refer the interested reader to the recent reviews listed below for other aspects of thin film simulation. General reviews for modeling the morphological evolution during epitaxial thin film growth may be found in Evans et al. [37] and in Makeev [80]. Tiedje & Ballestad [126] reviewed comparisons of experimental data, kinetic Monte-Carlo (kMC) simulations and continuum growth models for thin film epitaxy. A review of kMC methods in materials modeling may be found in Chatterjee & Vlachos [24]. Caflisch [18] reviewed the use of level-set methods and lattice models (kMC) for the dynamics of strained islands during epitaxy. Here, we discuss the finite element method applied to front-tracking methods, phase-field and level-set methods.

To illustrate how these methods work and to compare the methods with one another, we shall provide many examples of numerical simulations. Finally, we describe applications of these geometrical evolution laws to materials science problems. They include crystal growth from a bulk phase, the growth and morphologies of thin crystalline films with and without misfit strain, and applied external fields. We shall discuss instabilities in chemical vapor deposition (CVD), molecular beam epitaxy (MBE), liquid phase epitaxy (LPE), and electrodeposition.

The rest of the paper is organized as follows. In Section 2 we review the basic models of interface motion that include strong anisotropy and that are coupled with mass transport. In Section 3 we survey some of the new numerical methods developed for simulating the motion of isotropic interfaces and extend them to the general anisotropic case. In Section 4 we describe some applications of geometrical evolution laws and numerical methods to materials science problems, focusing mainly on thin films. Finally, in Section 5 we draw conclusions.

2 Anisotropic evolution laws in materials science

2.1 Classical models

The basic geometrical evolution laws in modeling material interfaces, such as grain boundaries, solid-liquid or solid-vapor interfaces, and domain boundaries in coherent phase transitions, are derived in Mullins [88, 89] and Herring [54, 55]. The partial differential equations for these evolution laws are given by the motion by mean curvature

$$V = -H \quad (2.1)$$

and the motion by the Laplacian of mean curvature

$$V = \Delta_{\Gamma} H, \quad (2.2)$$

respectively. Here $\Gamma = \Gamma(t)$ represents a moving material interface, treated as an oriented hypersurface in \mathbb{R}^{d+1} ($d = 1, 2$), V denotes the normal velocity of a point $\mathbf{x} = \mathbf{x}(t) \in \Gamma(t)$ defined by

$$V = \frac{d\mathbf{x}}{dt} \cdot \mathbf{n},$$

where $d\mathbf{x}/dt$ is the velocity of Γ and \mathbf{n} is the unit normal of Γ at \mathbf{x} at time t , H is the total curvature of Γ defined to be the sum of all the principal curvatures $\kappa_1, \dots, \kappa_d$, and Δ_{Γ} denotes the surface Laplacian. Note that the interface shape is independent of the choice of tangential velocity. Eq. (2.1), often called the mean-curvature flow (MCF), models the evaporation-condensation mechanism of a solid surface. Eq. (2.2) models surface diffusion. Note that in both models for the case $d = 2$, we have absorbed a factor of $1/2$ into the time scale as the mean curvature is actually defined as $H/2$.

Mathematically, these evolution laws are the L^2 and H^{-1} gradient flows, respectively, of a surface free energy functional

$$E[\Gamma] = \int_{\Gamma} \gamma_0 d\Gamma,$$

where γ_0 is a constant surface tension which we take to be 1 for mathematical convenience. As seen in the next section, the variational derivative of $E[\Gamma]$ with respect to Γ is given by

$$\frac{\delta E}{\delta \Gamma} = H$$

with respect to the L^2 norm and by

$$\frac{\delta E}{\delta \Gamma} = -\Delta_{\Gamma} H$$

with respect to the H^{-1} norm, respectively. Using steepest descent, we then have

$$V = -\frac{\delta E}{\delta \Gamma} = -H$$

and

$$V = -\frac{\delta E}{\delta \Gamma} = \Delta_{\Gamma} H,$$

respectively. For surface diffusion, one can also use the conservation of mass and the L^2 variation,

$$V + \nabla_{\Gamma} \cdot \mathbf{j} = 0 \quad \text{and} \quad \mathbf{j} = -\nabla_{\Gamma} \frac{\delta E}{\delta \Gamma} = -\nabla_{\Gamma} H$$

to derive Eq. (2.2), where \mathbf{j} denotes the surface flux, $\nabla_{\Gamma} \cdot$ is the surface divergence, and ∇_{Γ} is the surface gradient.

Another evolution law of interest in this class of models is the volume-conserved mean curvature flow

$$V = -(H - c) \tag{2.3}$$

with $c = \int_{\Gamma} H d\Gamma / \int_{\Gamma} d\Gamma$ the averaged mean curvature.

For applications in materials science, the surface tension is usually not a constant, but rather is a function of the orientation of the surface, reflecting the crystalline structure of an underlying material. In general, the surface energy reads

$$E[\Gamma] = \int_{\Gamma} \gamma d\Gamma$$

with $\gamma = \gamma(\mathbf{n})$ the surface tension, possibly depending on the normal to the surface \mathbf{n} . The geometric evolution laws can be again defined as gradient flows of the energy and

read (see the next subsection for a discussion of their variational derivation)

$$V = -kH_\gamma, \quad (2.4)$$

$$bV = -(H_\gamma - c), \quad (2.5)$$

$$V = \nabla_\Gamma \cdot (\nu \nabla_\Gamma H_\gamma), \quad (2.6)$$

respectively. Here $k = k(\mathbf{n})$ is the evaporation modulus, $b = b(\mathbf{n})$ is a kinetic coefficient, $\nu = \nu(\mathbf{n})$ denotes the surface mobility, H_γ is weighted mean curvature [20, 125]

$$H_\gamma = \nabla_\Gamma \cdot \zeta,$$

where the Cahn-Hoffman ζ -vector [20, 56, 125] is defined componentwise by $\zeta_i = \partial_{p_i} \gamma$ where ∂_{p_i} denotes the first derivative of the one-homogeneous extension of $\gamma: S^d \subset \mathbb{R}^{d+1} \rightarrow \mathbb{R}$ with respect to \mathbf{n} in the i th principal direction where S^d denotes the unit sphere of \mathbb{R}^{d+1} . Note that $H_\gamma = \frac{\delta E}{\delta \Gamma} \cdot \mathbf{n}$, the variational derivative of the anisotropic surface energy obtained by varying Γ in normal direction. The coefficient $c = \int_\Gamma b^{-1} H_\gamma d\Gamma / \int_\Gamma b^{-1} d\Gamma$ is an average of the weighted mean curvature.

Eq. (2.4) models the surface motion by evaporation-condensation and is known as anisotropic mean curvature flow, Eq. (2.5) describes the kinetics associated with the rearrangement of atoms on the surface and is known as volume conserved anisotropic mean curvature flow, Eq. (2.6) accounts for the diffusion of atoms along the surface and is known as motion by anisotropic surface diffusion.

A more general geometric evolution law combining all the three effects has been discussed by Fried and Gurtin [40]. The unified motion law is given by

$$V = \nabla_\Gamma \cdot (\nu \nabla_\Gamma (H_\gamma + bV)) - k(H_\gamma + bV). \quad (2.7)$$

We obtain the individual laws discussed above as follows:

- $\nu = 0, b = 0 \Rightarrow$ (2.4) for evaporation-condensation;
- $\nu = \infty, k = 0 \Rightarrow$ (2.5) for kinetics;
- $b = 0, k = 0 \Rightarrow$ (2.6) for surface diffusion.

The special case $k=0$ has been considered by Cahn and Taylor [22] and can also be written as

$$V = -(\nabla_\Gamma \cdot (\nu \nabla_\Gamma)) \left(\nabla \cdot (\nu \nabla_\Gamma) - \frac{1}{b} \right)^{-1} \left(\frac{1}{b} H_\gamma \right). \quad (2.8)$$

Setting $\nu = 0$ in Eq. (2.7) gives

$$\left(\frac{1}{k} + b \right) V = -H_\gamma, \quad (2.9)$$

which again is a curvature flow equation, but with a modified kinetic coefficient. If we set $b = 0$ in Eq. (2.7) we obtain a combined law for surface diffusion and evaporation-condensation

$$V = \nabla_\Gamma \cdot (\nu \nabla_\Gamma H_\gamma) - kH_\gamma. \quad (2.10)$$

2.2 Variational derivation

A variational derivation of Eq. (2.7) has been recently given in [120]. We briefly present a derivation of this equation here. Without any contribution from the bulk phases we can define for the normal velocity V

$$bV = -\frac{\delta E}{\delta \Gamma}$$

with $b = b(\mathbf{n})$ a non-negative kinetic coefficient. This evolution defines a gradient flow and thus guarantees thermodynamic consistency. But the evolution of the surface is also influenced from the bulk phases adjacent to the surface, e.g. solid and liquid, and thus we need also to consider the jump in the grand canonical potential of the bulk phases, see Cermelli and Jabbour [23]: $\Psi^+ - \rho^+ \mu^+ - \Psi^- + \rho^- \mu^-$, with Ψ^\pm the free energy density in the solid and liquid, ρ^\pm the density in the solid and liquid and μ^\pm the chemical potential in the solid and liquid, respectively. The surface evolution equation now reads

$$bV = -\frac{\delta E}{\delta \Gamma} - \Psi^+ + \rho^+ \mu^+ + \Psi^- - \rho^- \mu^-.$$

This incorporates effects from both the surface and the bulk. Assume the solid is unconstrained. Then the limiting value of the chemical potential at the surface is equal to the surface chemical potential $\mu = \mu^+$.

We now consider mass conservation. To derive this we take an interfacial pillbox along an arbitrary subsurface $\Sigma = \Sigma(t)$ of the interface $\Gamma(t)$, see Fig. 1. The subsurface $\Sigma(t)$ has the geometric boundary $\partial\Sigma$. Due to the interaction with the bulk phases the pillbox also has to have boundaries with the solid phase, namely Σ^+ and with the liquid phase Σ^- , again see Fig. 1.

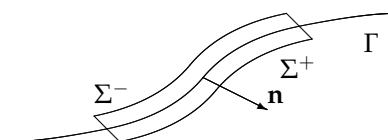


Figure 1: Schematic of an interfacial pillbox along the interface, here shown as a curve. Let $\Sigma(t)$ be an evolving subsurface of $\Gamma(t)$ whose geometric boundary is $\partial\Sigma$. Adapting the approach of Fried and Gurtin [40] to surfaces, we view the interfacial pillbox as encapsulating $\Sigma(t)$ and having an infinitesimal thickness. The pillbox boundary then consists of (i) two surfaces, one with unit normal $\mathbf{n}(t)$ and lying in the liquid/vapor phase $\Sigma^-(t)$, the other with unit normal $-\mathbf{n}(t)$ and lying within the solid phase $\Sigma^+(t)$, and (ii) end faces which we identify with $\partial\Sigma(t)$.

The atomic balance on the pillbox requires that any change in surface mass m is only due to a surface flux \mathbf{q} across $\partial\Sigma$ and adsorption/desorption from the bulk phases F^\pm across Σ^\pm . We therefore have

$$\frac{d}{dt}m = -\int_{\partial\Sigma} \mathbf{q} \cdot \mathbf{m} ds + \int_{\Sigma} F d\Gamma,$$

with $F = F^+ + F^-$ and \mathbf{m} the conormal. Due to the movement of Σ we also have

$$\frac{d}{dt}m = \int_{\Sigma} \rho V d\Gamma,$$

with $\rho = \rho^+$ the bulk density in the solid and V the normal velocity of Σ . Together with the formula for integration by parts on Σ we obtain

$$\int_{\partial\Sigma} \mathbf{q} \cdot \mathbf{m} ds = \int_{\Sigma} \nabla_{\Gamma} \cdot \mathbf{q} d\Gamma.$$

This leads to the local mass balance law

$$\rho V = -\nabla_{\Gamma} \cdot \mathbf{q} + F.$$

We now need to define constitutive equations for \mathbf{q} and F . For \mathbf{q} , we take

$$\mathbf{q} = -v \nabla_{\Gamma} \mu,$$

with $v = v(\mathbf{n})$ a non-negative coefficient, corresponding to surface diffusivity. For F , we take

$$F = -k^+(\mu - \mu^+) - k^-(\mu - \mu^-),$$

with $k^{\pm} = k^{\pm}(\mathbf{n})$ non-negative coefficient, corresponding to attachment, see, e.g., [5, 15]. Again with the assumption of an unconstrained solid we have $\mu = \mu^+$.

In the following, unless otherwise stated, we neglect for simplicity all remaining contributions from the bulk phases. Thus we set $\mu^- = 0$, $\Psi^{\pm} = 0$ and obtain a coupled system of equations for the evolution of Γ

$$\rho V = \nabla_{\Gamma} \cdot (v \nabla_{\Gamma} \mu) - k^- \mu,$$

$$bV = -\frac{\delta E}{\delta \Gamma} + \rho \mu.$$

This is a general model to describe the evolution of homogeneous crystalline surfaces that incorporates different mass transport mechanisms on the surface, such as surface diffusion, attachment-detachment, and other kinetics due to the rearrangement of atoms on the surface. If we set $\rho = 1$ and $k^- = k$, and use $\frac{\delta E}{\delta \Gamma} = H_{\gamma}$, then we obtain

$$V = \nabla_{\Gamma} \cdot (v \nabla_{\Gamma} \mu) - k \mu, \quad (2.11)$$

$$bV = -H_{\gamma} + \mu. \quad (2.12)$$

This is exactly Eq. (2.7) with $\mu = H_{\gamma} + bV$ introduced in order to write the fourth order equation as a system of second order equations.

2.3 Influence of the kinetic term

In most discussions on mass transport on materials surfaces the kinetic term bV is neglected. But even if b is small the effect might still be relevant as discussed in [40]. If we assume ν and b to be constant, Eq. (2.7) can be written as

$$V - \nu b \Delta_{\Gamma} V + kbV = \nu \Delta_{\Gamma} H_{\gamma} - kH_{\gamma}.$$

Thus, whether or not the kinetic term is important depends on the magnitude of the products νb and kb and not only b . The numerical solutions provided in Sec. 3 later will further indicate the importance of the kinetic term.

2.4 Strong anisotropy: regularization

Experimental studies show faceting of metal surfaces. One example of thermal faceting is observed by oxygen-absorption of $Cu(115)$ surfaces, see Reinecke and Taglauer [99]. Similar results can be obtained for Pd adsorbate on $W(111)$ surfaces, see Szczepkiewicz *et al.* [124]. The observed hill-valley topography coarsens but the size of facets does not exceed a limit of several nm . This is due to kinetic limitations. The equilibrium shape can only be reached for small crystals. It is suspected that the effect of O_2 or Pd in these experiments might be a change in the surface free energy, which leads to an increase of the strength of the anisotropy and thus to non-convex functions.

A non-convex anisotropy function results in the development of corners and edges in the Wulff shape. The Wulff shapes may be plotted using the approach described by Sekerka [109]. Fig. 2 gives an example. In two-dimensions the difficulty with non-convex anisotropies is very apparent. Here the free energy can be expressed as a function of an angle $\gamma = \gamma(\theta)$ and the weighted mean curvature can be written as $H_{\gamma} = \tilde{\gamma}H$, with $\tilde{\gamma} = \gamma + \gamma''$ the stiffness, which becomes negative within the non-convex region. An example of such function is

$$\gamma(\theta) = 1 + \epsilon_6 \cos(6\theta)$$

with increasing values for ϵ_6 . If $\epsilon_6 > 1/35 \approx 0.02857$ the free energy becomes non-convex. Besides the speculated influence of the adsorbate on ϵ_6 , there is also evidence that pure materials show strong non-convex anisotropies. Recent analytical results in classical density functional theory (DFT) predict a functional dependence as described and estimate $\epsilon_6 = 0.04$ for Cu , see, e.g., [79]. Calculations within a phase-field crystal (PFC) approach furthermore show equilibrium shapes with faceted structure and thus further indicate a strong anisotropy in the free energy, see [4]. Mathematically such strong anisotropies, which lead to corners and edges in the equilibrium shapes of crystals, give rise to ill-posed evolution equations. This means that, for orientations within the non-convex region, the geometric evolution laws become backward parabolic.

One way to overcome the resulting inherently unstable behavior of the dynamics problem with a non-convex free energy is to regularize the equation by adding a curvature dependent term to the interface energy. This was already proposed on physical

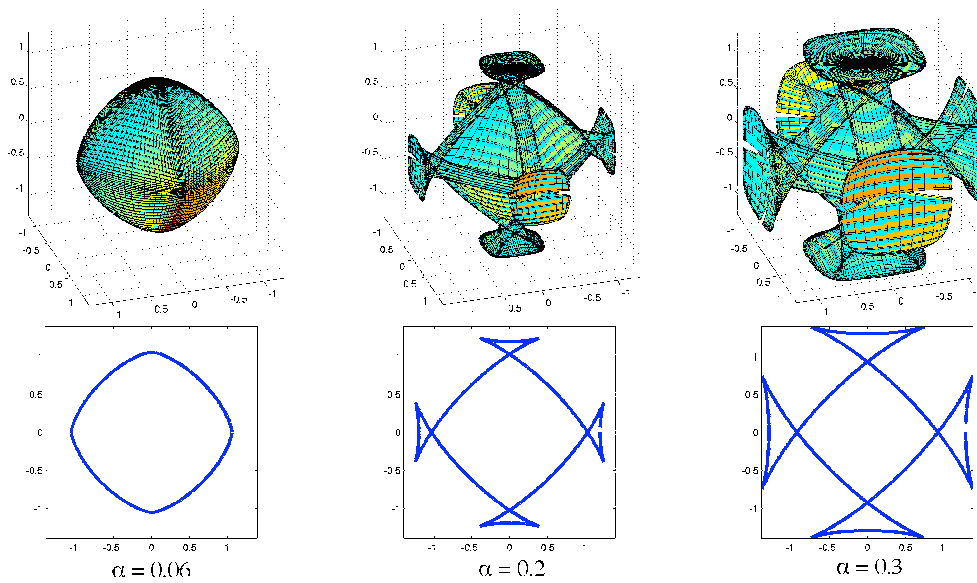


Figure 2: Wulff plot (ξ -plot) for a crystal with four-fold anisotropy [109].

grounds by Herring [53], and later mathematically introduced by DiCarlo et al. [29]. Such a curvature dependent term introduces a new length scale on which sharp corners are rounded. In two-dimensions the penalized interfacial energy density reads $\gamma_\alpha = \gamma + \frac{1}{2}\alpha^2\kappa^2$, with $\alpha > 0$ setting the length scale of the rounded corner, and κ denoting the curvature. Minimizing the surface energy

$$E_\alpha[\Gamma] = \int_\Gamma \gamma_\alpha ds$$

is therefore a compromise between a large curvature at the corner, which decreases orientations with large surface energy but increases the regularization term, and small curvature away from the corner which decreases the regularization term but increases orientations with large surface energy. The amount of corner rounding is therefore determined by these two competing energy terms.

The plausibility of such a regularization is clear, but its effect on the equilibrium shape has only been recently analyzed. Spencer [117] presents an asymptotic analysis that shows the convergence to the sharp-corner results as the regularization parameter $\alpha \rightarrow 0$. This therefore validates the use of such a regularization in numerical simulations and provides a mathematical basis for its use. With $\kappa = \partial_s \theta$ the regularized energy $E_\alpha[\Gamma]$ can also be interpreted as a geometric analog of a Ginzburg-Landau energy, see Hauser and Voigt [51].

For surfaces the free energy is generalized by Gurtin and Jabbour [46] to read

$$E_\alpha[\Gamma] = \int_\Gamma \gamma(\mathbf{n}) + \frac{1}{2}\alpha^2 H^2 d\Gamma. \quad (2.13)$$

A lack of regularity however indicates that even higher order term are needed in three

dimensions to prevent the solution from forming corners or edges, see Rätz and Voigt [98]. A general functional dependence of the surface free energy on such higher order terms, $\gamma_\alpha = \gamma(\mathbf{n}, H, \nabla_\Gamma H, \dots)$, can be found in the early work of Herring [53]. We will here discuss only the resulting evolution law if a curvature regularization is used as in (2.13). The variational derivative with respect to Γ reads

$$\frac{\delta E_\alpha}{\delta \Gamma} = H_\gamma - \alpha^2 \left(\Delta_\Gamma H + H \left(\|S\|^2 - \frac{1}{2} H^2 \right) \right),$$

with $S = \nabla_\Gamma \mathbf{n}$ being the shape operator and $\|S\| = \sqrt{\text{trace}(SS^T)}$ its Frobenius norm, see, e.g., Willmore [136]. Alternatively, we may also write

$$\|S\|^2 - \frac{1}{2} H^2 = \frac{1}{2} H^2 - 2K, \tag{2.14}$$

where K is the Gaussian curvature. The new set of equations thus read

$$V = \nabla_\Gamma \cdot (v \nabla_\Gamma \mu) - k\mu, \tag{2.15}$$

$$bV = -H_\gamma + \alpha^2 \left(\Delta_\Gamma H + H \left(\|S\|^2 - \frac{1}{2} H^2 \right) \right) + \mu. \tag{2.16}$$

This is a system of 6th order equations for the position vector \mathbf{x} of Γ . The special case of $v = b = \gamma = 0$ and $k = \alpha = 1$ reduces to the Willmore flow

$$V = \Delta_\Gamma H + H \left(\|S\|^2 - \frac{1}{2} H^2 \right)$$

whereas $k = b = \gamma = 0$ and $v = \alpha = 1$ can be interpreted as a conserved Willmore flow

$$V = -\Delta_\Gamma \left(\Delta_\Gamma H + H \left(\|S\|^2 - \frac{1}{2} H^2 \right) \right).$$

3 Numerical approaches

3.1 Front tracking by parametric finite elements

The basic idea of front tracking is to represent a moving front $\Gamma = \Gamma(t)$ at time t by a set of points $\mathbf{x}_i \in \Gamma(t)$ and move these points by a known normal velocity. This amounts to solving differential equations on the moving front.

3.1.1 Isotropic evolution

To formulate a front tracking approach, we follow the idea used by Bänsch et al. [6] to rewrite the higher order system as a system of 2nd and 0th order equations. To this end let us recall some identities in differential geometry. The mean curvature H is the trace of the shape operator $S = \nabla_\Gamma \mathbf{n}$, or equivalently the tangential divergence of the surface normal $H = \nabla_\Gamma \cdot \mathbf{n}$. It follows that

$$\Delta_\Gamma \mathbf{x} = -H\mathbf{n},$$

with \mathbf{x} being the position vector of a point on Γ . This is the starting point of a finite element discretization of mean curvature flow of parametric surfaces in [32] as it leads to the weak formulation

$$\int_{\Gamma} H\mathbf{n} \cdot \phi d\Gamma = \int_{\Gamma} \nabla_{\Gamma} \mathbf{x} \cdot \nabla_{\Gamma} \phi d\Gamma. \quad (3.1)$$

The isotropic case of (2.7) which reads

$$V = \nabla_{\Gamma} \cdot (v \nabla_{\Gamma} (H + bV)) - k(H + bV),$$

with v , b and k non-negative constants, can thus be rewritten as

$$\begin{aligned} \mathbf{H} &= -\Delta_{\Gamma} \mathbf{x}, \\ \mu &= bV + \mathbf{H} \cdot \mathbf{n}, \\ V &= \nabla_{\Gamma} \cdot (v \nabla_{\Gamma} \mu) - k\mu, \\ \mathbf{V} &= V\mathbf{n}, \end{aligned}$$

where we have used the mean curvature vector $\mathbf{H} = H\mathbf{n}$ and the normal velocity vector $\mathbf{V} = V\mathbf{n}$. Notice that we use $\mathbf{V} = V\mathbf{n}$ to define \mathbf{V} . This is not the velocity of a point at Γ . But the normal component of \mathbf{V} is exactly the same as that of the velocity, i.e.,

$$\mathbf{V} \cdot \mathbf{n} = \frac{d\mathbf{x}}{dt} \cdot \mathbf{n} = V.$$

If we now discretize in time, we can update the position vector \mathbf{x} in the first equation, such that

$$\mathbf{x}^{m+1} = \mathbf{x}^m + \tau_m \mathbf{V}^{m+1},$$

with τ_m the time step. This is Euler's method applied to the motion law $d\mathbf{x}/dt = \mathbf{V}$ which has the same normal velocity V and hence leads to the same location of surface at each time t . We thus obtain a coupled system for which a semi-implicit weak form reads

$$\begin{aligned} \int_{\Gamma^m} \mathbf{H}^{m+1} \phi d\Gamma - \tau_m \nabla_{\Gamma^m} \mathbf{V}^{m+1} \cdot \nabla_{\Gamma^m} \phi d\Gamma &= \int_{\Gamma^m} \nabla_{\Gamma^m} \mathbf{x}^m \cdot \nabla_{\Gamma^m} \phi d\Gamma, \\ \int_{\Gamma^m} \mu^{m+1} \phi d\Gamma - \int_{\Gamma^m} V^{m+1} \phi d\Gamma - \int_{\Gamma^m} \mathbf{H}^{m+1} \cdot \mathbf{n}^m \phi d\Gamma &= 0, \\ \int_{\Gamma^m} V^{m+1} \phi d\Gamma + \int_{\Gamma^m} \nabla_{\Gamma^m} \mu^{m+1} \cdot \nabla_{\Gamma^m} \phi d\Gamma + \int_{\Gamma^m} \mu^{m+1} \phi d\Gamma &= 0, \\ \int_{\Gamma^m} \mathbf{V}^{m+1} \phi d\Gamma - \int_{\Gamma^m} V^{m+1} \mathbf{n}^m \phi d\Gamma &= 0, \end{aligned}$$

where ϕ is a corresponding scalar or vectoral test function. The formulation now is implicit in the unknowns \mathbf{H}^{m+1} , μ^{m+1} , V^{m+1} and \mathbf{V}^{m+1} , but explicit in the geometric quantities Γ^m and \mathbf{n}^m , which leads to a linear system. To discretize in space, we use linear finite elements. We solve the resulting linear system of equation by a Schur-complement approach for V^{m+1} , from which \mathbf{V}^{m+1} is computed and $\mathbf{x}^{m+1} = \mathbf{x}^m + \tau_m \mathbf{V}^{m+1}$ is updated.

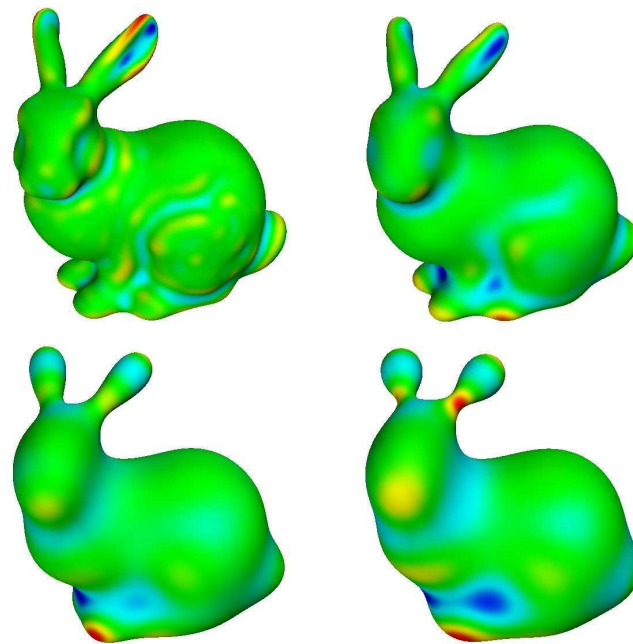


Figure 3: Surface evolution due to surface diffusion. Red indicates a normal velocity inwards and blue outwards. Simulations performed by F. Haußer [131].

Fig. 3 shows the evolution of the Stanford bunny under surface diffusion ($b=k=0, v=1$). The bunny thereby serves as an example of a complicated surface, with approximately 70,000 elements. In the simulation we use local mesh regularization and angle width control to prevent mesh distortion as well as time step control and adaptivity in space along the lines as described by Bänsch et al. [6]. The next example shows the evolution of an $8 \times 1 \times 1$ prism until a pinch-off, see Fig. 4.

3.1.2 Weak anisotropic surface free energy

The anisotropic case, with a weak anisotropy in the surface free energy, can be considered along the same lines and has been described by Haußer and Voigt [50]. An extension of (3.1) to the anisotropic case reads

$$\int_{\Gamma} H_{\gamma} \mathbf{n} \cdot \phi \, d\Gamma = \int_{\Gamma} \gamma(\mathbf{n}) \nabla_{\Gamma} \mathbf{x} \cdot \nabla_{\Gamma} \phi \, d\Gamma - \sum_{k,l=1}^3 \int_{\Gamma} \gamma_{z_k}(\mathbf{n}) \nabla_{\Gamma} x_k \cdot \nabla_{\Gamma} \phi_l \, d\Gamma,$$

where we have used the notation $\gamma_{z_k} = \zeta_k$, the k^{th} component of the Cahn-Hoffman ζ -vector [20, 56]. It is particularly interesting to note, that no second derivative of γ is involved in the weak form, so the only assumption we have on γ is convexity, to ensure the evolution laws to remain forward parabolic. We require

$$D^2\gamma(\mathbf{p}) \mathbf{q} \cdot \mathbf{q} \geq \gamma_0 \mathbf{q} \cdot \mathbf{q} \quad \forall \mathbf{p}, \mathbf{q} \in \mathbb{R}^3, \quad |\mathbf{p}|=1, \quad \mathbf{p} \cdot \mathbf{q}=0,$$

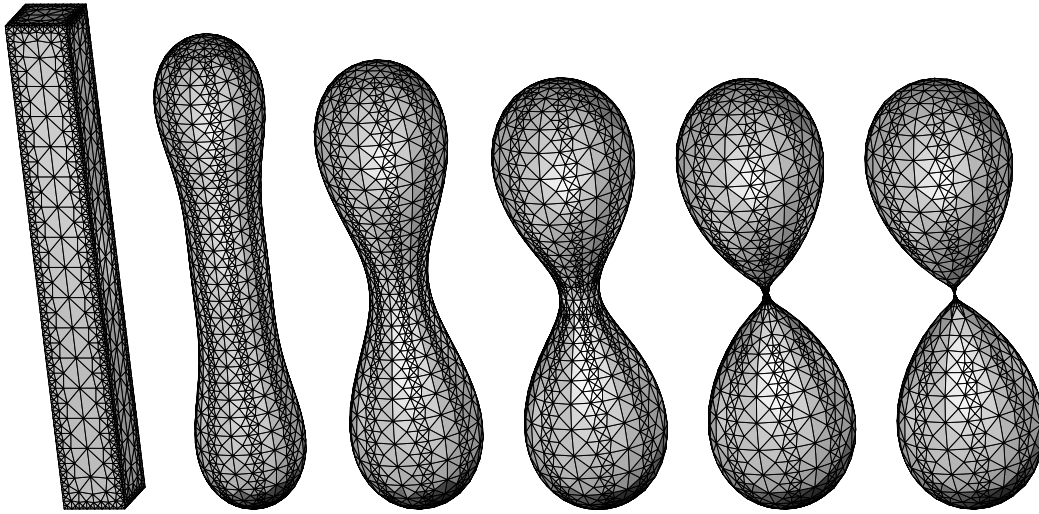


Figure 4: Surface evolution due to surface diffusion. Simulations performed by P. Morin [6].

with some $\gamma_0 > 0$. (This γ_0 may not be the usual constant surface tension.) We now rewrite Eq. (2.7) as

$$\begin{aligned} (\mathbf{H}_\gamma)_i &= -\nabla_\Gamma \cdot (\gamma(\mathbf{n}) \nabla_\Gamma x_i) + \sum_{k=1}^3 \nabla_\Gamma \cdot (\gamma_{z_k} n_i \nabla_\Gamma x_k), \quad i=1,2,3, \\ \mu &= bV + \mathbf{H}_\gamma \cdot \mathbf{n}, \\ V &= \nabla_\Gamma \cdot (\nu \nabla_\Gamma \mu) - k\mu, \\ \mathbf{V} &= V\mathbf{n}, \end{aligned}$$

where we have used the weighted curvature vector $\mathbf{H}_\gamma = H_\gamma \mathbf{n}$. Again discretizing in time and updating the position vector \mathbf{x} in the first equation, such that

$$\mathbf{x}^{m+1} = \mathbf{x}^m + \tau_m \mathbf{V}^{m+1},$$

leads to the semi-implicit weak form

$$\begin{aligned} & \int_{\Gamma^m} \mathbf{H}_\gamma^{m+1} \phi d\Gamma - \tau_m \gamma(\mathbf{n}^m) \nabla_{\Gamma^m} \mathbf{V}^{m+1} \cdot \nabla_{\Gamma^m} \phi d\Gamma \\ &= \int_{\Gamma^m} \gamma(\mathbf{n}^m) \nabla_{\Gamma^m} \mathbf{x}^m \cdot \nabla_{\Gamma^m} \phi d\Gamma - \sum_{k=1}^3 \int_{\Gamma^m} \gamma_{z_k}(\mathbf{n}^m) n_l^m \nabla_{\Gamma^m} x_k^m \cdot \nabla_{\Gamma^m} \phi_l d\Gamma, \\ & \int_{\Gamma^m} \mu^{m+1} \phi d\Gamma - \int_{\Gamma^m} b(\mathbf{n}^m) V^{m+1} \phi d\Gamma - \int_{\Gamma^m} \mathbf{H}_\gamma^{m+1} \cdot \mathbf{n}^m \phi d\Gamma = 0, \\ & \int_{\Gamma^m} V^{m+1} \phi d\Gamma + \int_{\Gamma^m} \nu(\mathbf{n}^m) \nabla_{\Gamma^m} \mu^{m+1} \cdot \nabla_{\Gamma^m} \phi d\Gamma + \int_{\Gamma^m} k(\mathbf{n}^m) \mu^{m+1} \phi d\Gamma = 0, \\ & \int_{\Gamma^m} \mathbf{V}^{m+1} \phi d\Gamma - \int_{\Gamma^m} V^{m+1} \mathbf{n}^m \phi d\Gamma = 0, \end{aligned}$$

where ϕ is a corresponding scalar or a vector test function.

Compared with the isotropic case, the anisotropy functions introduce additional nonlinearities. They can be treated in an explicit way. With such an explicit treatment the system may no longer be unconditionally stable, which is true for the isotropic case. Therefore we add the stabilizing term below, as used by Deckelnick et al. in [28], to the left hand side of the first equation

$$\begin{aligned}
 & -\tau_m \lambda \int_{\Gamma^m} \gamma(\mathbf{n}^m) \nabla_{\Gamma^m} (\mathbf{V}^{m+1} - \mathbf{V}^m) \cdot \nabla_{\Gamma^m} \phi \, d\Gamma \\
 & + \sum_{k,l=1}^3 \int_{\Gamma^m} \gamma_{z_k}(\mathbf{n}^m) \nabla_{\Gamma^m} (V_k^{m+1} - V_k^m) \cdot \nabla_{\Gamma^m} \phi \, d\Gamma.
 \end{aligned} \tag{3.2}$$

The formulation now is again implicit in the unknowns \mathbf{H}_γ^{m+1} , μ^{m+1} , V^{m+1} and \mathbf{V}^{m+1} , but explicit in the geometric quantities Γ^m and \mathbf{n}^m , which leads to a linear system.

To discretize in space, we again use linear finite elements and solve the resulting linear equation by a Schur-complement approach for V^{m+1} , from which \mathbf{V}^{m+1} is computed and $\mathbf{x}^{m+1} = \mathbf{x}^m + \tau_m \mathbf{V}^{m+1}$ is updated.



Figure 5: Wulff shape W_γ for regularized l^1 -anisotropy, with $W_\gamma = \{\mathbf{z} \in \mathbb{R}^3 \mid \mathbf{z} \cdot \mathbf{q} \leq \gamma(\mathbf{z}) \, \forall \mathbf{q} \in \mathbb{R}^3\}$.

We apply our algorithm to the evolution of a surface under a regularized l^1 -anisotropy

$$\gamma(\mathbf{z}) = \sum_{k=1}^3 \sqrt{0.01|\mathbf{z}|^2 + z_k^2}.$$

The corresponding Wulff shape is depicted in Fig. 5. Fig. 6 shows the evolution of a sphere towards the Wulff shape if $b = 0$, $k = 0$ and $\nu = 1$.

3.1.3 Strong anisotropic surface free energy

To deal with strong (non-convex) anisotropies in γ is more involved. A front tracking approach for these higher order equations has only been introduced for curves by Siegel

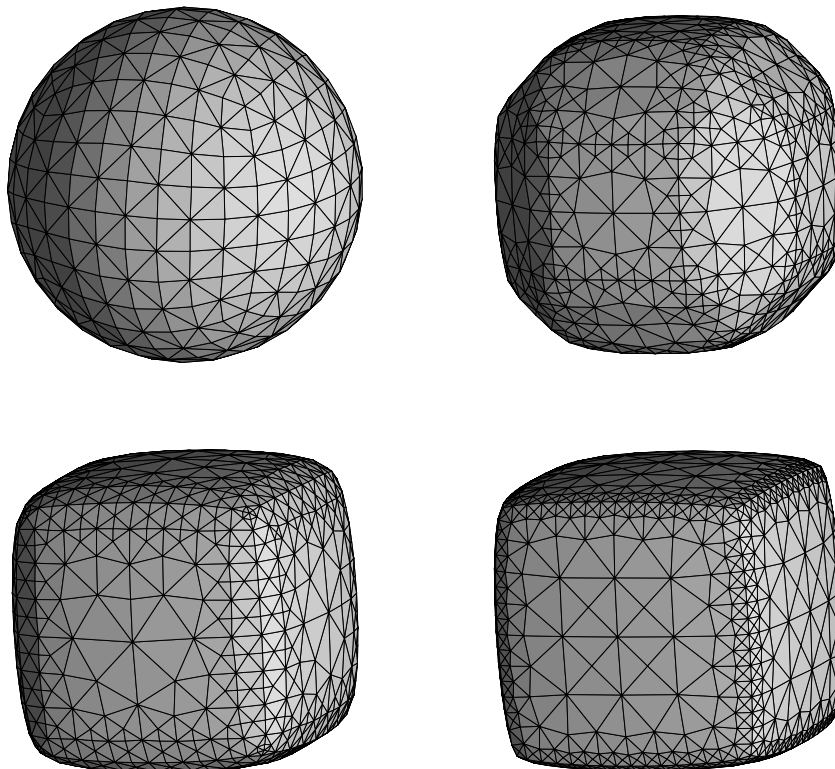


Figure 6: Evolution of a sphere towards its steady state. Refinement in regions of high curvature and coarsening in nearly flat regions. The final number of grid points is 1085. Simulations performed by F. Hauser [50].

et al. [110] and Hauser and Voigt [47,49]. An extension to surfaces will require an efficient treatment of $\|S\|^2$. This problem is addressed in an approach for Willmore flow by Rusu [105], see also Deckelnick et al. [27]. We will adapt this approach here and combine it with the approach for the weak anisotropic evolution discussed in the previous section.

We now rewrite Eqs. (2.15)-(2.16) as

$$\begin{aligned}
 \mathbf{H} &= -\Delta_{\Gamma} \mathbf{x}, \\
 (\mathbf{H}_{\gamma})_i &= -\nabla_{\Gamma} \cdot (\gamma(\mathbf{n}) \nabla_{\Gamma} x_i) + \sum_{k=1}^3 \nabla_{\Gamma} \cdot (\gamma_{z_k} n_i \nabla_{\Gamma} x_k), \quad i=1,2,3, \\
 \mu &= bV + \mathbf{H}_{\gamma} \cdot \mathbf{n} - \alpha^2 \omega, \\
 \omega &= \Delta_{\Gamma} H + H \left(\|S\|^2 - \frac{1}{2} H^2 \right), \\
 V &= \nabla_{\Gamma} \cdot (v \nabla_{\Gamma} \mu) - k\mu, \\
 \mathbf{V} &= V \mathbf{n},
 \end{aligned}$$

where we have again used the curvature and weighted curvature vector $\mathbf{H} = H\mathbf{n}$ and $\mathbf{H}_\gamma = H_\gamma\mathbf{n}$, respectively, and introduced the new variable ω . Using the trick of Rusu [105] a weak form for

$$\omega = \Delta_\Gamma H + H \left(\|S\|^2 - \frac{1}{2}H \right)$$

can be written as

$$\int_{\Gamma^m} \omega \phi d\Gamma = \int_{\Gamma^m} \mathbf{R}(\mathbf{n}) \nabla_\Gamma \mathbf{H} \cdot \nabla_\Gamma \phi d\Gamma - \frac{1}{2} \int_{\Gamma^m} \|\mathbf{H}\|^2 \nabla_\Gamma \mathbf{x} \cdot \nabla_\Gamma \phi d\Gamma$$

with $\mathbf{R} = R_{kl}$ and $R_{kl} = \delta_{kl} - 2n_k n_l$. Again discretization in time and updating the position vector \mathbf{x} , such that

$$\mathbf{x}^{m+1} = \mathbf{x}^m + \tau_m \mathbf{V}^{m+1},$$

lead to a semi-implicit discretization, which reads in a weak form

$$\begin{aligned} & \int_{\Gamma^m} \mathbf{H}^{m+1} \phi d\Gamma - \tau_m \int_{\Gamma^m} \nabla_{\Gamma^m} \mathbf{V}^{m+1} \cdot \nabla_{\Gamma^m} \phi d\Gamma = \int_{\Gamma^m} \nabla_{\Gamma^m} \mathbf{x}^m \cdot \nabla_{\Gamma^m} \phi d\Gamma, \\ & \int_{\Gamma^m} \mathbf{H}_\gamma^{m+1} \phi d\Gamma - \tau_m \int_{\Gamma^m} \gamma(\mathbf{n}^m) \nabla_{\Gamma^m} \mathbf{V}^{m+1} \cdot \nabla_{\Gamma^m} \phi d\Gamma \\ & = \int_{\Gamma^m} \gamma(\mathbf{n}^m) \nabla_{\Gamma^m} \mathbf{x}^m \cdot \nabla_{\Gamma^m} \phi d\Gamma - \sum_{k=1}^3 \int_{\Gamma^m} \gamma_{z_k}(\mathbf{n}^m) n_l^m \nabla_{\Gamma^m} x_k^m \cdot \nabla_{\Gamma^m} \phi_l d\Gamma, \\ & \int_{\Gamma^m} \mu^{m+1} \phi d\Gamma - \int_{\Gamma^m} b(\mathbf{n}^m) V^{m+1} \phi d\Gamma - \int_{\Gamma^m} \mathbf{H}_\gamma^{m+1} \cdot \mathbf{n}^m \phi d\Gamma + \int_{\Gamma^m} \alpha \omega^{m+1} \phi d\Gamma = 0, \\ & \int_{\Gamma^m} \omega^{m+1} \phi d\Gamma - \frac{\tau_m}{2} \int_{\Gamma^m} \|\mathbf{H}^m\|^2 \nabla_{\Gamma^m} \mathbf{V}^{m+1} \cdot \nabla_{\Gamma^m} \phi d\Gamma - \int_{\Gamma^m} \mathbf{R}(\mathbf{n}^m) \nabla_{\Gamma^m} \mathbf{H}^{m+1} \cdot \nabla_{\Gamma^m} \phi d\Gamma \\ & + \frac{1}{2} \int_{\Gamma^m} \|\mathbf{H}^m\|^2 \nabla_{\Gamma^m} \mathbf{x}^m \cdot \nabla_{\Gamma^m} \phi d\Gamma = 0, \\ & \int_{\Gamma^m} V^{m+1} \phi d\Gamma + \int_{\Gamma^m} \nu(\mathbf{n}^m) \nabla_{\Gamma^m} \mu^{m+1} \cdot \nabla_{\Gamma^m} \phi d\Gamma + \int_{\Gamma^m} k(\mathbf{n}^m) \mu^{m+1} \phi d\Gamma = 0, \\ & \int_{\Gamma^m} \mathbf{V}^{m+1} \phi d\Gamma - \int_{\Gamma^m} V^{m+1} \mathbf{n}^m \phi d\Gamma = 0, \end{aligned}$$

where ϕ is a corresponding scalar or vectoral test function. Again the stabilization term (3.2) should be added to the second equation above.

An implementation of this algorithm for surfaces is not yet available. Detailed studies concerning the evolution towards the Wulff shape for closed curves as well as coarsening dynamics of curves have been considered with the same algorithm restricted to curves in Hausser and Voigt [47] and [48], respectively.

3.2 Phase-field approximations

Instead of using an explicit description of the surface, we now represent the surface as the 1/2 level-set of auxiliary, phase-field function ϕ , which is defined in $\Omega \subset \mathbb{R}^{d+1}$; ϕ

is approximately 1 and 0 away from the interface with a rapid transition between the two occurring in a narrow region around the interface. The phase-field function ϕ is the solution to an appropriate evolution equation in the entire region Ω .

Phase-field models are widely used to describe complex evolution of patterns, see McFadden [83] and Emmerich [36] for recent reviews on its use in solidification and condensed-matter physics, respectively.

3.2.1 Isotropic evolution

In a similar way as shown in Section 2.2 we can derive the phase-field equation from the free energy

$$E[\phi] = \int_{\Omega} \frac{\epsilon}{2} |\nabla \phi|^2 + \frac{1}{\epsilon} G(\phi) d\Omega,$$

with $\epsilon > 0$ defining the width of the interfacial layer (diffuse interface) and

$$G(\phi) = 18\phi^2(1-\phi)^2$$

a double-well potential with minima in the two phases 0 and 1. Here $\nabla \phi$ is the usual gradient vector of ϕ with its i th component $\partial_{x_i} \phi$. The term $(\epsilon/2)|\nabla \phi|^2$ penalizes the transition from one phase to another and determines the size of transition region. The variational derivative of $E[\phi]$ reads

$$\frac{\delta E}{\delta \phi} = -\epsilon \Delta \phi + \frac{1}{\epsilon} G'(\phi).$$

Two well known equations are the Allen-Cahn equation

$$\partial_t \phi = -\frac{\delta E}{\delta \phi} \Rightarrow \partial_t \phi = \epsilon \Delta \phi - \frac{1}{\epsilon} G'(\phi)$$

and the Cahn-Hilliard equation

$$\partial_t \phi = -\nabla \cdot \mathbf{j}, \quad \mathbf{j} = -\nabla \frac{\delta E}{\delta \phi} \Rightarrow \partial_t \phi = \Delta \left(-\epsilon \Delta \phi + \frac{1}{\epsilon} G'(\phi) \right).$$

The phase-field approximation for the isotropic version of (2.7) reads

$$\partial_t \phi = \nabla \cdot \left(\nu \frac{1}{\epsilon} B(\phi) \nabla \left(-\epsilon \Delta \phi + \frac{1}{\epsilon} G'(\phi) + b \partial_t \phi \right) \right) - k \left(-\epsilon \Delta \phi + \frac{1}{\epsilon} G'(\phi) + b \partial_t \phi \right)$$

or rewritten as a system of two 2nd order equations

$$\partial_t \phi = \nabla \cdot \left(\nu \frac{1}{\epsilon} B(\phi) \nabla \mu \right) - k \mu, \tag{3.3}$$

$$b \partial_t \phi = \epsilon \Delta \phi - \frac{1}{\epsilon} G'(\phi) + \mu, \tag{3.4}$$

with ν, k, b non-negative constants, and the mobility function

$$B(\phi) = 36\phi^2(1-\phi)^2,$$

which restricts the diffusion to the diffuse interface. We consider the following special cases:

- $\nu = 0, b = 0 \Rightarrow$ Allen-Cahn equation

$$\partial_t \phi = k \left(\epsilon \Delta \phi - \frac{1}{\epsilon} G'(\phi) \right);$$

- $k = 0, b = 0 \Rightarrow$ degenerate Cahn-Hilliard equation

$$\partial_t \phi = \nabla \cdot \left(\nu \frac{1}{\epsilon} B(\phi) \nabla \mu \right),$$

$$0 = \epsilon \Delta \phi - \frac{1}{\epsilon} G'(\phi) + \mu;$$

- $k = 0, \nu = \infty \Rightarrow$ non-local Allen-Cahn

$$b \partial_t \phi = \epsilon \Delta \phi - \frac{1}{\epsilon} G'(\phi) + \frac{1}{\epsilon} \frac{\int_{\Omega} G'(\phi) dx}{\int_{\Omega} 1 dx};$$

- $k = 0 \Rightarrow$ viscous degenerate Cahn-Hilliard equation

$$\partial_t \phi = \nabla \cdot \left(\nu \frac{1}{\epsilon} B(\phi) \nabla \mu \right),$$

$$b \partial_t \phi = \epsilon \Delta \phi - \frac{1}{\epsilon} G'(\phi) + \mu;$$

- $\nu = 0 \Rightarrow$ Allen-Cahn equation

$$\left(\frac{1}{k} + b \right) \partial_t \phi = \epsilon \Delta \phi - \frac{1}{\epsilon} G'(\phi).$$

The above equations formally converge for $\epsilon \rightarrow 0$ to the following sharp interface laws:

- Allen-Cahn equation $\Rightarrow V = -kH$, see Evans et al. [38];
- degenerate Cahn-Hilliard equation $\Rightarrow V = \nabla_{\Gamma} \cdot (\nu \nabla_{\Gamma} H)$, see Cahn et al. [19];
- non-local Allen-Cahn $\Rightarrow bV = -(H - c)$, see Rubinstein and Sternberg [104];
- viscous degenerate Cahn-Hilliard equation $\Rightarrow V = \nabla_{\Gamma} \cdot (\nu \nabla_{\Gamma} (H + bV))$, see Elliott and Garcke [35];
- Allen-Cahn equation $\Rightarrow \left(\frac{1}{k} + b \right) V = -H$, Evans et al. [38].

More recent investigations on the case of surface diffusion indicate that the system

$$\partial_t \phi = \nabla \cdot \left(v \frac{1}{\epsilon} B(\phi) \nabla \mu \right) - k \mu, \quad (3.5)$$

$$b g(\phi) \partial_t \phi = \epsilon \Delta \phi - \frac{1}{\epsilon} G'(\phi) + \mu, \quad (3.6)$$

with

$$g(\phi) \approx \phi^2 (1 - \phi)^2$$

might even give a better asymptotic behavior than the standard approach in Eqs. (3.3)-(3.4), see Rätz et al. [97] and Müller-Gugenberger et al. [87].

For numerical approach for phase-field models we again refer to McFadden [83] and the references therein. Especially for the Allen-Cahn equation also a posteriori error estimates have been derived by Kesser et al. [64] and the convergence of adaptive finite element solutions to the solution for mean curvature flow could be shown by Feng and Prohl [39].

We will modify an approach for the degenerate Cahn-Hilliard equation to numerically solve Eqs. (3.3)-(3.4). Therefore we introduce a semi-implicit time-discretization, in which we linearize the double well as

$$\begin{aligned} G'(\phi^{m+1}) &\approx G'(\phi^m) + G''(\phi^m)(\phi^{m+1} - \phi^m) \\ &= G''(\phi^m)\phi^{m+1} + G'(\phi^m) - G''(\phi^m)\phi^m \end{aligned}$$

and obtain the following weak formulation

$$\begin{aligned} \int_{\Omega} \frac{\phi^{m+1} - \phi^m}{\tau_m} \psi \, d\Omega &= - \int_{\Omega} v \frac{1}{\epsilon} B(\phi^m) \nabla \mu^{m+1} \cdot \nabla \psi \, d\Omega - \int_{\Omega} k \mu^{m+1} \psi \, d\Omega, \\ \int_{\Omega} b \frac{\phi^{m+1} - \phi^m}{\tau_m} \psi \, d\Omega &= - \int_{\Omega} \epsilon \nabla \phi^{m+1} \cdot \nabla \psi \, d\Omega - \int_{\Omega} \frac{1}{\epsilon} G''(\phi^m) \phi^{m+1} \psi \, d\Omega \\ &\quad + \int_{\Omega} \frac{1}{\epsilon} (G'(\phi^m) - G''(\phi^m) \phi^m) \psi \, d\Omega + \int_{\Omega} \mu^{m+1} \psi \, d\Omega, \end{aligned}$$

with test functions $\psi \in \mathbb{R}^3$. The system is now linear in the unknowns ϕ^{m+1} and μ^{m+1} and is discretized in space by linear finite elements.

Adaptivity in space and time is used in all simulations. Fig. 7 shows the same problem as considered in Fig. 4. Here the $\frac{1}{2}$ -level-set of ϕ is shown for $k=0$, $b=0.001$ and $v=1$. The results nicely agree with those of the front tracking approach. The pinch-off time deviates by only 7.8% compared to the pinch-off reported by Bänsch et al. [6].

To demonstrate the importance of the kinetic coefficient b , we perform the same simulations but with an enhanced value of b . The evolution qualitatively changes if we increase the dependence of the kinetic coefficient. With $k=0$, $b=0.1$ and $v=1$ there is no pinch-off, see Fig. 8.

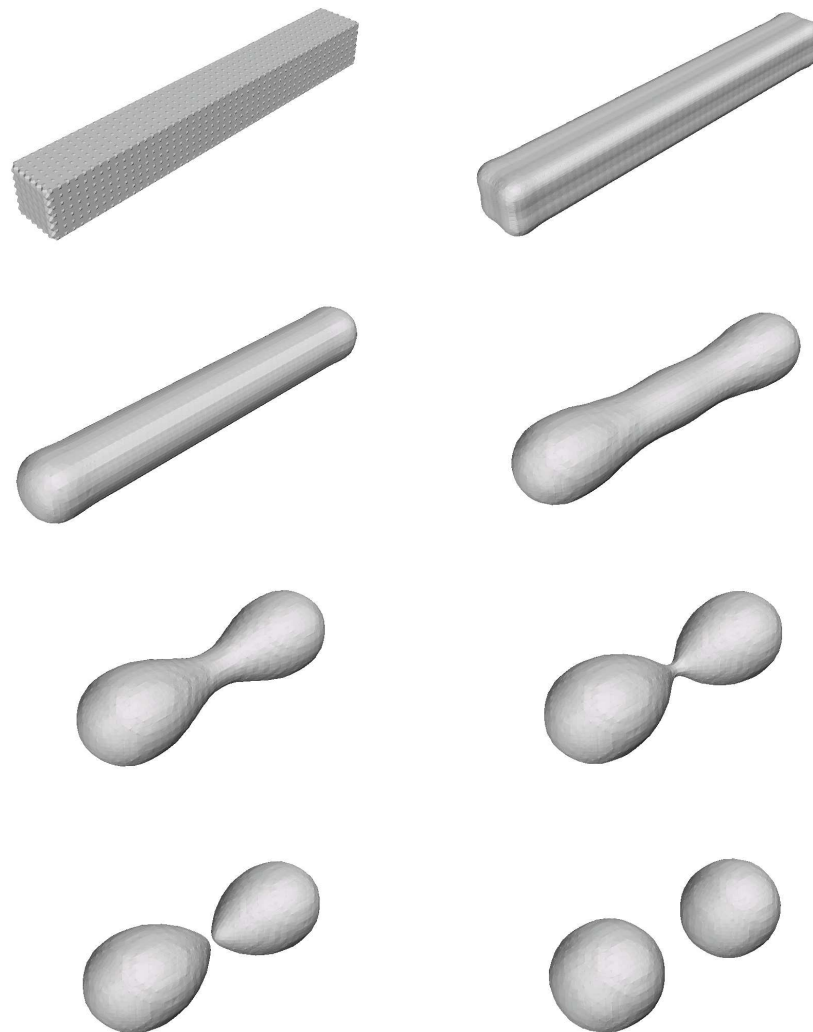


Figure 7: Phase-field approximations of surface evolution due to surface diffusion. Simulations performed by A. Rätz [96].

3.2.2 Weak anisotropic surface free energy

To consider the evolution in the anisotropic situation requires some care. Typically the energy is rewritten as [65]

$$E[\phi] = \int_{\Omega} \frac{\epsilon}{2} |\gamma \nabla \phi|^2 + \frac{1}{\epsilon} G(\phi) d\Omega, \tag{3.7}$$

with

$$\gamma = \gamma(\mathbf{n}), \quad \mathbf{n} = -\nabla \phi / |\nabla \phi|.$$

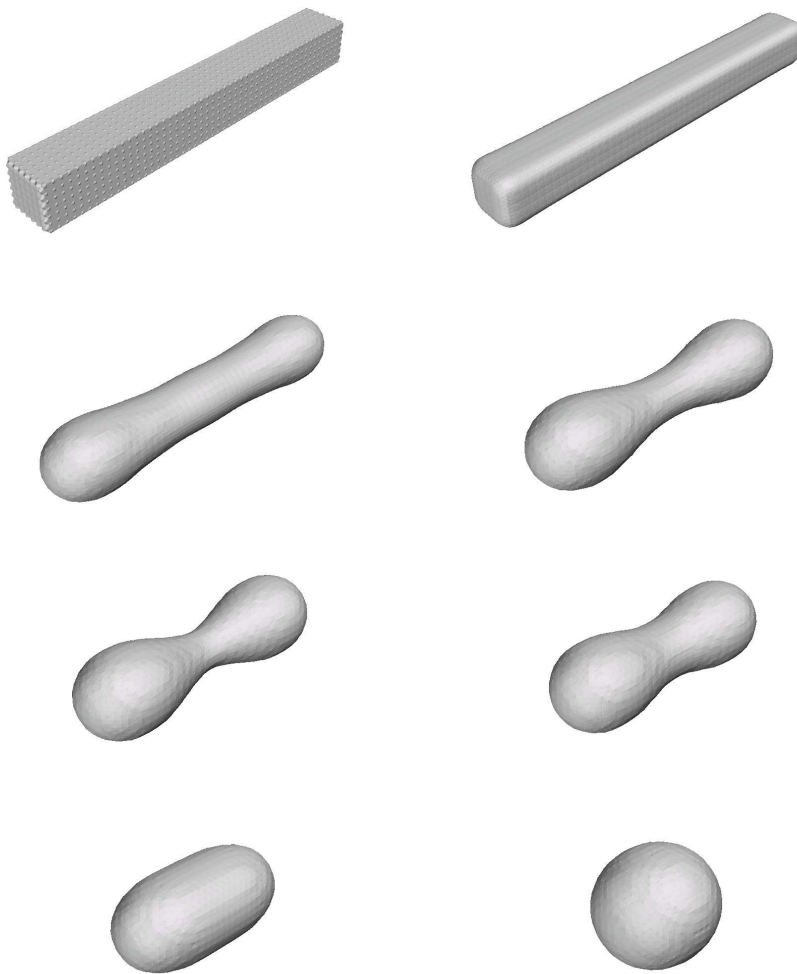


Figure 8: Phase-field approximations of surface evolution due to surface diffusion with kinetics. Simulations performed by A. Rätz [96].

In order to ensure the existence of the energy we assume for the one-homogeneous extension of γ

$$\gamma_0(\mathbf{p}) = \gamma\left(-\frac{\mathbf{p}}{|\mathbf{p}|}\right)|\mathbf{p}|, \quad \text{if } \mathbf{p} \neq 0$$

and $\gamma_0(\mathbf{0}) = 0$. The corresponding phase-field approximation then reads

$$\partial_t \phi = \nabla \cdot \left(\tilde{v} \frac{1}{\epsilon} B(\phi) \nabla \mu \right) - \tilde{k} \mu, \quad (3.8)$$

$$\tilde{b} \partial_t \phi = \epsilon \nabla \cdot (\gamma \nabla \phi + \gamma |\nabla \phi|^2 \nabla_{\nabla \phi} \gamma) - \frac{1}{\epsilon} G'(\phi) + \mu, \quad (3.9)$$

with $\tilde{v} = v/\gamma$, $\tilde{k} = k/\gamma$, $\tilde{b} = b/\gamma$ rescaled anisotropic coefficients. See Rätz et al. [97] for an asymptotic expansion to show the convergence to the sharp interface limit if $k = 0$. Other approaches in which either only an anisotropy in γ or b have been considered can be found in McFadden et al. [84], Cahn and Taylor [21] and Uehara and Sekerka [130], respectively. Faceted interfaces were considered using a phase-field approach by Debierre et al. [26].

The numerical approach is similar to the isotropic case:

$$\begin{aligned} & \int_{\Omega} \frac{\phi^{m+1} - \phi^m}{\tau_m} \psi \, d\Omega \\ &= - \int_{\Omega} \tilde{v}(\mathbf{n}^m) \frac{1}{\epsilon} B(\phi^m) \nabla \mu^{m+1} \cdot \nabla \psi \, d\Omega - \int_{\Omega} \tilde{k}(\mathbf{n}^m) \mu^{m+1} \psi \, d\Omega, \\ & \int_{\Omega} \tilde{b}(\mathbf{n}^m) \frac{\phi^{m+1} - \phi^m}{\tau_m} \psi \, d\Omega \\ &= - \int_{\Omega} \epsilon (\gamma(\mathbf{n}^n) \nabla \phi^{m+1} + \gamma(\mathbf{n}^m) |\nabla \phi^m|^2 \nabla_{\nabla \phi} \gamma(\mathbf{n}^m)) \cdot \nabla \psi \, d\Omega \\ & \quad - \int_{\Omega} \frac{1}{\epsilon} G''(\phi^m) \phi^{m+1} \psi \, d\Omega + \int_{\Omega} \frac{1}{\epsilon} (G'(\phi^m) - G''(\phi^m) \phi^m) \psi \, d\Omega + \int_{\Omega} \mu^{m+1} \psi \, d\Omega. \end{aligned}$$

All additional nonlinear terms, introduced by the anisotropy functions, are treated in an explicit way.

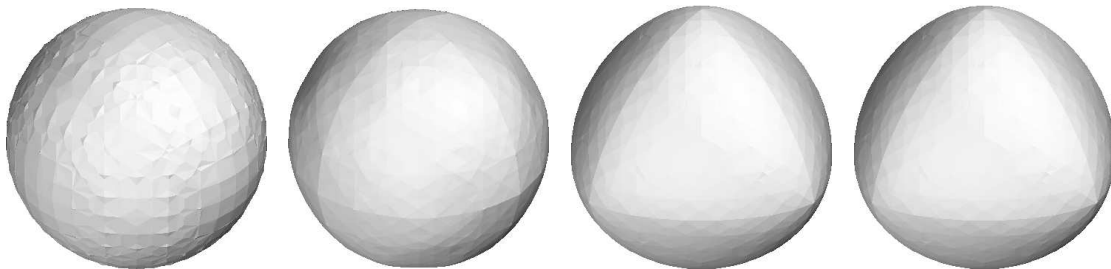


Figure 9: Diffuse interface approximation of surface evolution due to kinetic surface diffusion. Simulations performed by A. Rätz [97].

Fig. 9 shows the evolution of the 1/2 level-set of ϕ from a sphere towards the Wulff shape if

$$\gamma(\mathbf{n}) = 1 + 0.3 \sum_{i=1}^3 n_i^4,$$

$k = 0$, $b = 1$ and $v = 1$. One drawback of this classical way to incorporate anisotropy in the phase-field model, is that the width of the diffuse interface depends on the interface orientation, e.g. \mathbf{n} . Even if this may be physically correct on an atomistic scale, using the phase-field approach as a numerical tool with a larger interface thickness, the variable interface thickness introduces incompatibility between anisotropic and isotropic components of the system. One consequence is that this formulation requires the rescaling of

the coefficients in Eqs. (3.8)-(3.8). This becomes particularly complicated when the phase-field approximation of the Willmore energy is incorporated, as described below.

An alternative way to incorporate anisotropy has recently been proposed by Torabi et al. [127]. Comparing the sharp interface and diffuse interface free energy in the isotropic situation

$$E[\Gamma] = \int_{\Gamma} 1 d\Gamma \quad \text{and} \quad E[\phi] = \int_{\Omega} 1 \left(\frac{\epsilon}{2} |\nabla \phi|^2 + \frac{1}{\epsilon} G(\phi) \right) d\Omega.$$

Note that $(\frac{\epsilon}{2} |\nabla \phi|^2 + \frac{1}{\epsilon} G(\phi)) d\Omega$ can be interpreted as an approximation of the area element $d\Gamma$. Thus an appropriate relation in the anisotropic situation reads

$$E[\Gamma] = \int_{\Gamma} \gamma(\mathbf{n}) d\Gamma \quad \text{and} \quad E[\phi] = \int_{\Omega} \gamma(\mathbf{n}) \left(\frac{\epsilon}{2} |\nabla \phi|^2 + \frac{1}{\epsilon} G(\phi) \right) d\Omega,$$

with $\mathbf{n} = -\nabla \phi / |\nabla \phi|$ in the diffuse interface free energy formulation. The evolution equation based on this energy now reads

$$\partial_t \phi = \nabla \cdot \left(\nu \frac{1}{\epsilon} B(\phi) \nabla \mu \right) - k\mu, \quad (3.10)$$

$$b \partial_t \phi = \epsilon \nabla \cdot (\gamma \nabla \phi) + \nabla \cdot \left(\left(\frac{\epsilon}{2} |\nabla \phi|^2 + \frac{1}{\epsilon} G(\phi) \right) \nabla_{\nabla \phi} \gamma \right) - \frac{1}{\epsilon} \gamma G'(\phi) + \mu. \quad (3.11)$$

A matched asymptotic analysis for surface diffusion ($k=0$, $b=0$ and $\nu=1$) is shown in Torabi et al. [127]. In contrast to the previous formulation no rescaling of the anisotropy functions k , b and ν is required. Furthermore the formulation ensures a constant diffuse interface width, only depending on ϵ .

For the numerical treatment we again use a semi-implicit time-discretization in which all anisotropy functions are treated explicitly

$$\begin{aligned} & \int_{\Omega} \frac{\phi^{m+1} - \phi^m}{\tau_m} \psi d\Omega \\ &= - \int_{\Omega} \nu(\mathbf{n}^m) \frac{1}{\epsilon} B(\phi^m) \nabla \mu^{m+1} \cdot \nabla \psi d\Omega - \int_{\Omega} k(\mathbf{n}^m) \mu^{m+1} \psi d\Omega, \\ & \int_{\Omega} b(\mathbf{n}^m) \frac{\phi^{m+1} - \phi^m}{\tau_m} \psi d\Omega \\ &= - \int_{\Omega} \epsilon \gamma(\mathbf{n}^m) \nabla \phi^{m+1} \cdot \nabla \psi d\Omega + \int_{\Omega} \left(\frac{\epsilon}{2} |\nabla \phi^m|^2 + \frac{1}{\epsilon} G(\phi) \right) \nabla_{\nabla \phi} \gamma(\mathbf{n}^m) \cdot \nabla \psi d\Omega \\ & \quad - \int_{\Omega} \frac{1}{\epsilon} \gamma(\mathbf{n}^m) G''(\phi^m) \phi^{m+1} \psi d\Omega + \int_{\Omega} \frac{1}{\epsilon} \gamma(\mathbf{n}^m) \left(G'(\phi^m) - G''(\phi^m) \phi^m \right) \psi d\Omega + \int_{\Omega} \mu^{m+1} \psi d\Omega. \end{aligned}$$

3.2.3 Strong anisotropic surface free energy

To derive a phase-field approximation for Eqs. (2.15)-(2.16) we first need to generalize the free energy in (3.7) and add an appropriate approximation for the curvature regularization term. Proposed diffuse interface approximations for the Willmore energy go back to

DiGiorgi [42]. An appropriate form would read

$$E_{reg}[\phi] = \frac{1}{2} \int_{\Omega} \left(-\epsilon \Delta \phi + \frac{1}{\epsilon} G'(\phi) \right)^2 \left(\frac{\epsilon}{2} |\phi|^2 + \frac{1}{\epsilon} G(\phi) \right) d\Omega, \tag{3.12}$$

where $(-\epsilon \Delta \phi + \frac{1}{\epsilon} G'(\phi))^2$ gives an approximation of H^2 and

$$\frac{\epsilon}{2} |\gamma \phi|^2 + \frac{1}{\epsilon} G(\phi) d\Omega$$

approximates the area element $d\Gamma$. An alternate approach has been used by Biben and Misbah [10], see also [9,59], where the curvature is calculated directly by $H = \nabla \cdot \mathbf{n}$ and the integrand of Eq. (3.12) is replaced by $H^2 |\nabla \phi|$ where $|\nabla \phi|$ approximates the area element $d\Gamma$. Another related regularization of the strongly anisotropic phase-field system consists of replacing E_{reg} above by $\delta^2 / 2 \int_{\Omega} |\Delta \phi|^2 d\Omega$. This Laplacian-squared regularization was investigated by Wise et al. [138], Wheeler [134] and Wise et al. [137].

In Loretti and March [78], Du et al. [31] and Rösler and Schätzle [101] it is shown that the energy can be simplified to

$$E_{reg}[\phi] = \frac{1}{2} \int_{\Omega} \frac{1}{\epsilon} \left(-\epsilon \Delta \phi + \frac{1}{\epsilon} G'(\phi) \right)^2 d\Omega,$$

which leads to the following evolution equation for a diffuse interface approximation of Willmore flow

$$\begin{aligned} \partial_t \phi &= \Delta \omega - \frac{1}{\epsilon^2} G''(\phi) \omega, \\ \omega &= -\epsilon \Delta \phi + \frac{1}{\epsilon} G'(\phi), \end{aligned}$$

and of conserved Willmore flow

$$\begin{aligned} \partial_t \phi &= \nabla \cdot \left(\frac{1}{\epsilon} B(\phi) \nabla \mu \right), \\ \mu &= -\Delta \omega + \frac{1}{\epsilon^2} G''(\phi) \omega, \\ \omega &= -\epsilon \Delta \phi + \frac{1}{\epsilon} G'(\phi). \end{aligned}$$

A matched asymptotic analysis for the first equation showing the convergence to Eq. (2.4) was given by Loretti and March [78]. The DiGiorgi approach has an advantage over the Biben and Misbah approach in that the DiGiorgi energy explicitly forces the phase-field function to acquire its asymptotic form to a higher order in ϵ . That is,

$$\phi \sim q(d/\epsilon) + \mathcal{O}(\epsilon^2),$$

where q is the transition function across the diffuse interface (e.g. hyperbolic tangent) and d is the signed distance to the interface [31]. The corresponding dynamics using

the Laplacian-squared regularization [134, 137, 138] does not converge to Willmore flow because the Laplacian of ϕ does not fully approximate the interface curvature.

A naive approach to an appropriate free energy thus would be to add the two energies

$$E_\alpha[\phi] = E[\phi] + \alpha^2 E_{reg}[\phi],$$

as proposed by Rätz et al. [97]. A matched asymptotic analysis of the resulting equations however fails to converge to (2.15)-(2.16). This is because of the incompatibility between the anisotropic (surface energy) and the isotropic (Willmore energy) components of the energy. In particular, the Willmore energy forces the interface thickness to be uniform which is incompatible with the original form of the anisotropic surface energy. To get the asymptotics right the anisotropy has to be incorporated also in $E_{reg}[\phi]$. An appropriate form for the energy suggested by Röger [100] then reads

$$E_\alpha[\phi] = \int_\Omega \frac{\epsilon}{2} |\gamma \nabla \phi|^2 + \frac{1}{\epsilon} G'(\phi) + \frac{\alpha^2}{2} \frac{1}{\gamma \epsilon} \left(-\gamma \epsilon \Delta \phi + \frac{1}{\gamma \epsilon} G'(\phi) \right)^2 d\Omega.$$

An alternative method is to follow the idea of Torabi et al. [127] and use

$$E_\alpha[\phi] = \int_\Omega \gamma(\mathbf{n}) \left(\frac{\epsilon}{2} |\nabla \phi|^2 + \frac{1}{\epsilon} G(\phi) \right) + \frac{\alpha^2}{2} \frac{1}{\epsilon} \left(-\epsilon \Delta \phi + \frac{1}{\epsilon} G'(\phi) \right)^2 d\Omega,$$

which does not require a rescaling of the Willmore energy and thus leads to the much simpler set of evolution equations

$$\partial_t \phi = \nabla \cdot \left(v \frac{1}{\epsilon} B(\phi) \nabla \mu \right) - k \mu, \quad (3.13)$$

$$b \partial_t \phi = \epsilon \nabla \cdot (\gamma \nabla \phi) + \nabla \cdot \left(\left(\frac{\epsilon}{2} |\nabla \phi|^2 + \frac{1}{\epsilon} G(\phi) \right) \nabla_{\nabla \phi} \gamma \right) - \frac{1}{\epsilon} \gamma G'(\phi) + \mu + \alpha^2 \left(\Delta \omega - \frac{1}{\epsilon^2} G''(\phi) \omega \right), \quad (3.14)$$

$$\omega = -\epsilon \Delta \phi + \frac{1}{\epsilon} G'(\phi). \quad (3.15)$$

In Torabi et al. [127] a matched asymptotic analysis shows the convergence to Eqs. (2.15)-(2.16) as $\epsilon \rightarrow 0$.

The numerical approach now reads

$$\begin{aligned} & \int_\Omega \frac{\phi^{m+1} - \phi^m}{\tau_m} \psi d\Omega \\ &= - \int_\Omega v(\mathbf{n}^m) \frac{1}{\epsilon} B(\phi^m) \nabla \mu^{m+1} \cdot \nabla \psi d\Omega - \int_\Omega k(\mathbf{n}^m) \mu^{m+1} \psi d\Omega, \end{aligned}$$

$$\begin{aligned}
 & \int_{\Omega} b(\mathbf{n}^m) \frac{\phi^{m+1} - \phi^m}{\tau_m} \psi \, d\Omega \\
 = & - \int_{\Omega} \epsilon \gamma(\mathbf{n}^m) \nabla \phi^{m+1} \cdot \nabla \psi \, d\Omega + \int_{\Omega} \left(\frac{\epsilon}{2} |\nabla \phi^m|^2 + \frac{1}{\epsilon} G(\phi) \right) \nabla_{\nabla \phi} \gamma(\mathbf{n}^m) \cdot \nabla \psi \, d\Omega \\
 & - \int_{\Omega} \frac{1}{\epsilon} \gamma(\mathbf{n}^m) G''(\phi^m) \phi^{m+1} \psi \, d\Omega + \int_{\Omega} \frac{1}{\epsilon} \gamma(\mathbf{n}^m) \left(G'(\phi^m) - G''(\phi^m) \phi^m \right) \psi \, d\Omega \\
 & + \int_{\Omega} \mu^{m+1} \psi \, d\Omega - \int_{\Omega} \alpha^2 \nabla \omega^{m+1} \cdot \nabla \psi \, d\Omega - \int_{\Omega} \alpha^2 \frac{1}{\epsilon^2} G''(\phi^m) \omega^{m+1} \, d\Omega, \\
 & \int_{\Omega} \omega^{m+1} \psi \, d\Omega \\
 = & \int_{\Omega} \epsilon \nabla \phi^{m+1} \cdot \nabla \psi \, d\Omega + \int_{\Omega} \frac{1}{\epsilon} G''(\phi^m) \phi^{m+1} \psi \, d\Omega + \int_{\Omega} \frac{1}{\epsilon} \left(G'(\phi^m) - G''(\phi^m) \phi^m \right) \psi \, d\Omega.
 \end{aligned}$$

The system can be solved by linear finite elements using adaptivity in space and time and a multigrid method to solve the linear equations.

In Fig. 10, the evolution of a sphere towards the Wulff shape is shown using the adaptive finite difference method described in [127] for the strongly anisotropic system with $b = k = 0$. It can be shown [117, 127] that by decreasing α the solutions converge to the Wulff shape in Fig. 2. In Fig. 11, the thermal faceting and subsequent coarsening of strongly anisotropic film in an unstable orientation is shown. In both of these simulations, the rounding of corners and edges is clearly visible. Within the film evolution we observe first the nucleation of facets as a result of the decomposition process. The subsequent coarsening is a result of the edge energy associated with the $\frac{\alpha^2}{2} H^2$ term, which is reduced if the number of transitions between the stable facet orientations is reduced.

3.3 The level-set approach

The level-set method, first introduced in [90], is a computational technique for tracking evolving surfaces. The starting point of this method is to describe a moving surface $\Gamma = \Gamma(t)$ at time t implicitly as the 0 level-set of an auxiliary function $\phi = \phi(\mathbf{x}, t)$, i.e., $\Gamma(t) = \{\mathbf{x} : \phi(\mathbf{x}, t) = 0\}$. For instance, if Γ is a three-dimensional surface (such as a sphere) then the function $\phi(\mathbf{x}, t)$ at any time t is a function defined on the three-dimensional space, i.e., \mathbf{x} has three coordinates. We shall call ϕ a level-set function of Γ . This level-set function evolves according to

$$\partial_t \phi + V \|\nabla \phi\| = 0,$$

where V is the normal velocity. This basic equation, often called the level-set equation, can be derived by simply taking the time derivative of the equation $\phi(\mathbf{x}(t), t) = 0$, using the chain rule and the definition of normal velocity. The normal velocity V needs to be extended off the surface so that the level-set equation can be solved in an appropriate space domain.

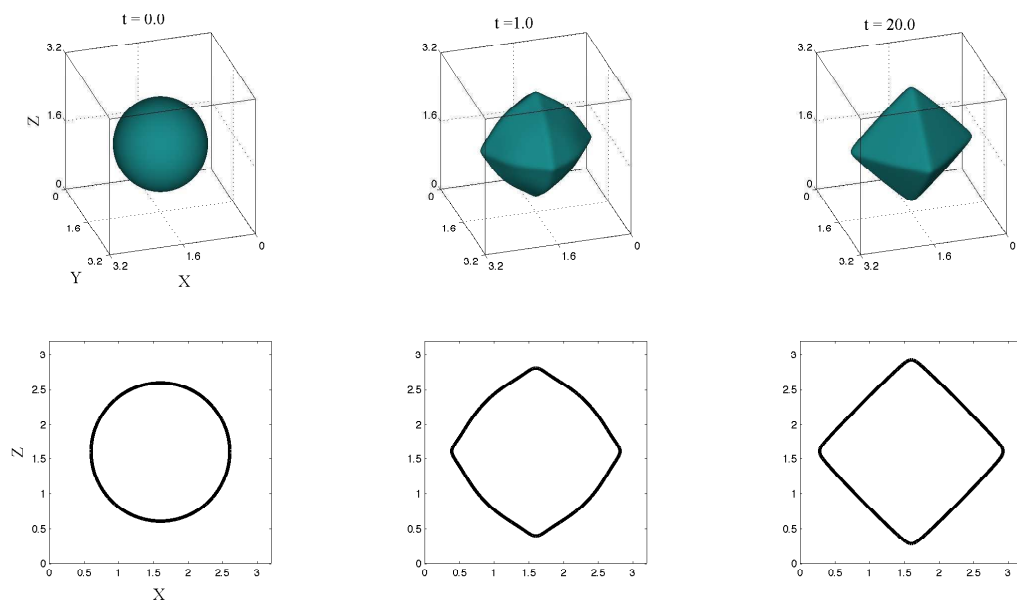


Figure 10: Evolution towards the Wulff shape. Top: the 0.5 isosurface of ϕ . Bottom: a slice through the center showing the 0.5 contour line. Simulations are performed by S. Torabi [127].

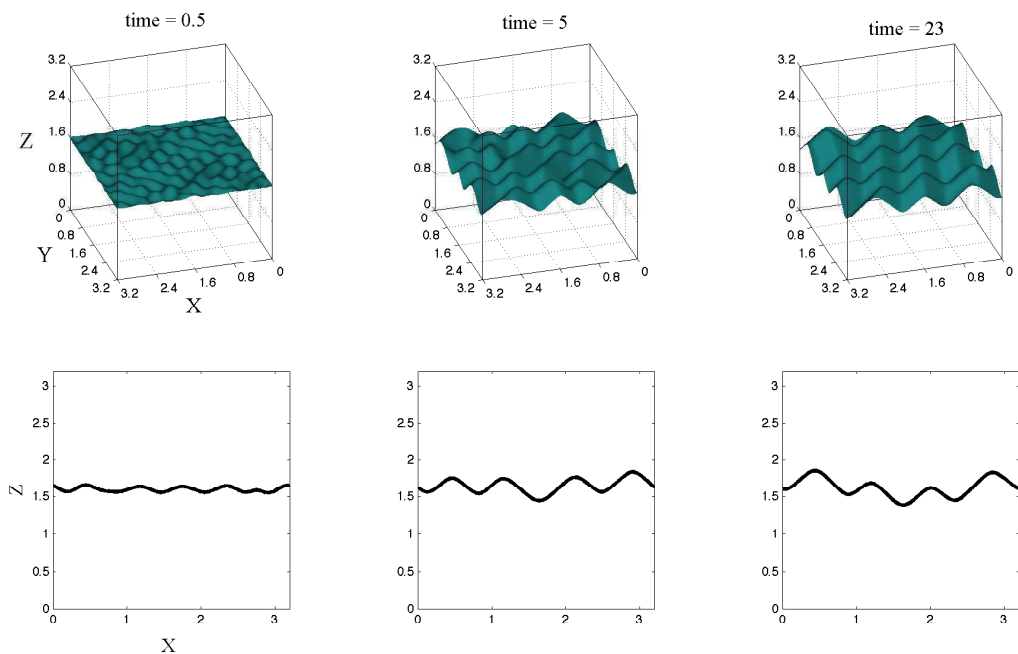


Figure 11: Thermal faceting of an unstable orientation and subsequent coarsening of surface structures. Simulations are performed by S. Torabi [127].

3.3.1 Isotropic evolution

The normal and the mean curvature can be expressed as $\mathbf{n} = \nabla\phi/|\nabla\phi|$ and $H = \nabla \cdot \nabla\phi/|\nabla\phi|$, respectively. Using this, and

$$V = -\frac{\partial_t\phi}{\|\nabla\phi\|} \quad \text{and} \quad \nabla_\Gamma \cdot (v\nabla_\Gamma\mu) = \frac{1}{\|\nabla\phi\|} \nabla \cdot (v\mathbf{P}_{\nabla\phi}\nabla\mu)$$

with $\mathbf{P}_{\nabla\phi} = \mathbf{I} - \mathbf{n} \otimes \mathbf{n}$, we can reformulate Eq. (2.7) in the isotropic case, to obtain

$$\begin{aligned} -\partial_t\phi &= \nabla \cdot (v\|\nabla\phi\|\mathbf{P}_{\nabla\phi}\nabla\mu) - k\|\nabla\phi\|\mu, \\ -b\frac{\partial_t\phi}{\|\nabla\phi\|} &= -\nabla \cdot \frac{\nabla\phi}{\|\nabla\phi\|} + \mu, \end{aligned}$$

which gives a 4th-order equation for ϕ .

Levelset formulations for mean curvature flow and surface diffusion have been discussed in [25, 114]. Following the approach of [25] a semi-implicit time-discretization for the level-set formulation reads

$$\begin{aligned} -\int_\Omega \frac{\phi^{m+1} - \phi^m}{\tau_m} \psi \, d\Omega &= -\int_\Omega v\|\nabla\phi^m\|\mathbf{P}_{\nabla\phi^m}\nabla\mu^{m+1} \cdot \nabla\psi \, d\Omega - \int_\Omega k\|\nabla\phi^m\|\mu^{m+1}\psi \, d\Omega, \\ \int_\Omega \frac{b}{\|\nabla\phi^m\|} \frac{\phi^{m+1} - \phi^m}{\tau_m} \psi \, d\Omega &= -\int_\Omega \frac{\nabla\phi^{m+1}}{\|\nabla\phi^m\|} \cdot \nabla\psi \, d\Omega - \int_\Omega \mu^{m+1}\psi \, d\Omega. \end{aligned}$$

The resulting system is linear in the unknowns ϕ^{m+1} and μ^{m+1} and can be discretized in space by linear finite elements. Adaptivity in space and time is used to ensure efficient computation. The resulting system is solved by a Schur complement approach, see [25] for details. Fig. 12 shows the evolution towards a sphere if $k=0$, $b=0$ and $v=1$.

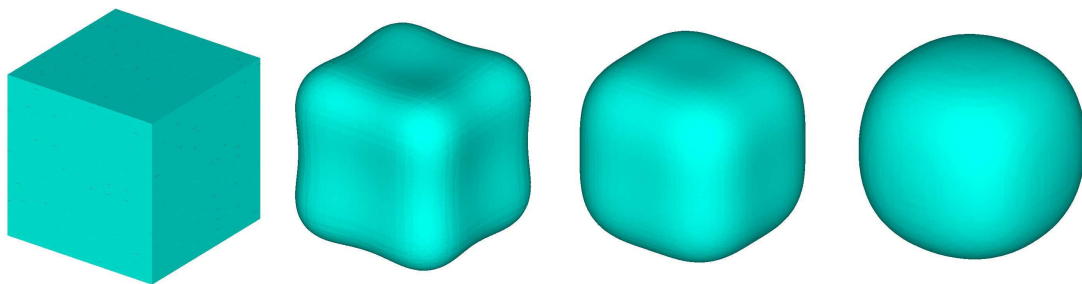


Figure 12: Levelset computation of surface evolution due to surface diffusion. Simulations performed by C. Stöcker [13].

3.3.2 Weak anisotropic surface free energy

An extension to the anisotropic situation reads

$$\begin{aligned} - \int_{\Omega} \frac{\phi^{m+1} - \phi^m}{\tau_m} \psi d\Omega &= - \int_{\Omega} \nu(\mathbf{n}^m) \|\nabla \phi^m\| \mathbf{P}_{\nabla \phi} \nabla \mu^{m+1} \cdot \nabla \psi d\Omega \\ &\quad - \int_{\Omega} k(\mathbf{n}^m) \|\nabla \phi^m\| \mu^{m+1} \psi d\Omega, \\ \int_{\Omega} \frac{b(\mathbf{n}^m)}{\|\nabla \phi^m\|} \frac{\phi^{m+1} - \phi^m}{\tau_m} \psi d\Omega &= - \int_{\Omega} \gamma_z \left(\frac{\nabla \phi^m}{\|\nabla \phi^m\|} \right) \cdot \nabla \psi d\Omega - \int_{\Omega} \mu^{m+1} \psi d\Omega. \end{aligned}$$

Again the additional non-linear terms are treated explicitly. We further add, as in the front tracking approach, a stabilization term to the right hand side

$$+ \int_{\Omega} \frac{\lambda}{\|\nabla \phi^m\|} \gamma \left(\frac{\nabla \phi^m}{\|\nabla \phi^m\|} \right) (\nabla \phi^{m+1} - \nabla \phi^m) \cdot \nabla \psi d\Omega,$$

which reduces for $\lambda = 1$ and an isotropic situation to the semi-implicit formulation in the isotropic case. The stabilization term was first introduced in [28]. The formulation is again linear and can be solved along the lines as the isotropic case. For a computational example see Fig. 13. It should be noted, also the level-set formulation does not require the surface free energy density to be smooth as the weak form uses only the first derivative.

3.3.3 Strong anisotropic surface free energy

To derive a level-set representation of Eqs. (2.15)-(2.16) we follow Burger et al. [13] and combine the previous formulation with a level-set approach for Willmore flow introduced by Droske and Rumpf [30]. The weak form then reads

$$\begin{aligned} - \int_{\Omega} \partial_t \phi \psi d\Omega &= - \int_{\Omega} \nu(\mathbf{n}) \|\nabla \phi\| \mathbf{P}_{\nabla \phi} \nabla \mu \cdot \nabla \psi d\Omega - \int_{\Omega} k(\mathbf{n}) \|\nabla \phi\| \mu \psi d\Omega, \\ \int_{\Omega} \frac{b(\mathbf{n})}{\|\nabla \phi\|} \partial_t \phi \psi d\Omega &= - \int_{\Omega} \gamma_z \left(\frac{\nabla \phi}{\|\nabla \phi\|} \right) \cdot \nabla \psi d\Omega - \int_{\Omega} \mu \psi d\Omega \\ &\quad + \int_{\Omega} \frac{\alpha^2}{2} \frac{(\omega)^2}{\|\nabla \phi\|^3} \nabla \phi \cdot \nabla \psi d\Omega + \int_{\Omega} \alpha^2 \frac{1}{\|\nabla \phi\|} \mathbf{P}_{\nabla \phi} \nabla \omega \cdot \nabla \psi d\Omega, \\ \int_{\Omega} \frac{\omega}{\|\nabla \phi\|} \psi d\Omega &= \int_{\Omega} \frac{\nabla \phi}{\|\nabla \phi\|} \cdot \nabla \psi d\Omega, \end{aligned}$$

and splits the 6th order equation into a system of 2nd order problems for ϕ , μ and ω .

The convexity splitting approach introduced by Burger et al. [13], and studied in more

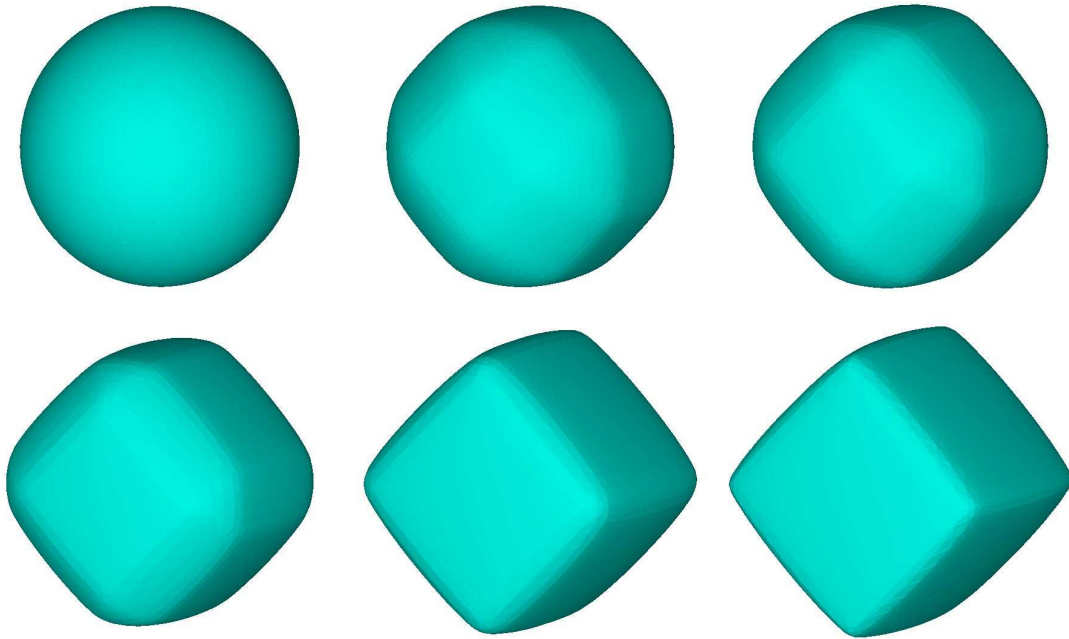


Figure 13: Levelset computation of surface evolution due to anisotropic surface diffusion. Simulations performed by C. Stöcker [13].

detail by Burger et al. [14], now leads to a semi-implicit time-discretization of the form

$$\begin{aligned}
 & - \int_{\Omega} \frac{\phi^{m+1} - \phi^m}{\tau_m} \psi \, d\Omega \\
 = & - \int_{\Omega} v(\mathbf{n}^m) \|\nabla \phi^m\| \mathbf{P}_{\nabla \phi} \nabla \mu^{m+1} \cdot \nabla \psi \, d\Omega - \int_{\Omega} k(\mathbf{n}^m) \|\nabla \phi^m\| \mu^{m+1} \psi \, d\Omega, \\
 & \int_{\Omega} \frac{b(\mathbf{n}^m)}{\|\nabla \phi^m\|} \frac{\phi^{m+1} - \phi^m}{\tau_m} \psi \, d\Omega \\
 = & - \int_{\Omega} \gamma_z \left(\frac{\nabla \phi^m}{\|\nabla \phi^m\|} \right) \cdot \nabla \psi \, d\Omega + \int_{\Omega} \frac{\lambda}{\|\nabla \phi^m\|} \gamma \left(\frac{\nabla \phi^m}{\|\nabla \phi^m\|} \right) (\nabla \phi^{m+1} - \nabla \phi^m) \cdot \nabla \psi \, d\Omega \\
 & - \int_{\Omega} \mu^{m+1} \psi \, d\Omega + \int_{\Omega} \frac{\alpha^2}{2} \frac{(\omega^m)^2}{\|\nabla \phi^m\|^3} \nabla \phi^{m+1} \cdot \nabla \psi \, d\Omega \\
 & + \int_{\Omega} \alpha^2 \frac{1}{\|\nabla \phi^m\|} \nabla \omega^{m+1} \cdot \nabla \psi \, d\Omega - \int_{\Omega} \alpha^2 \frac{\nabla \omega^m \cdot \nabla \phi^m}{\|\nabla \phi^m\|^3} \nabla \phi^m \cdot \nabla \psi \, d\Omega, \\
 & \int_{\Omega} \frac{\omega^{m+1}}{\|\nabla \phi^m\|} \psi \, d\Omega = \int_{\Omega} \frac{\nabla \phi^{m+1}}{\|\nabla \phi^m\|} \cdot \nabla \psi \, d\Omega,
 \end{aligned}$$

which uses the same stabilizing term as the weakly anisotropic formulation.

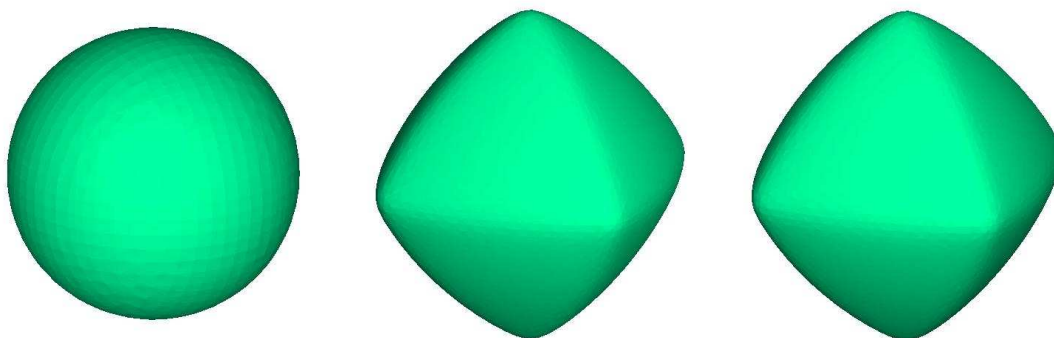


Figure 14: Convergence towards the Wulff shape. Simulations are performed by C. Stöcker [13].

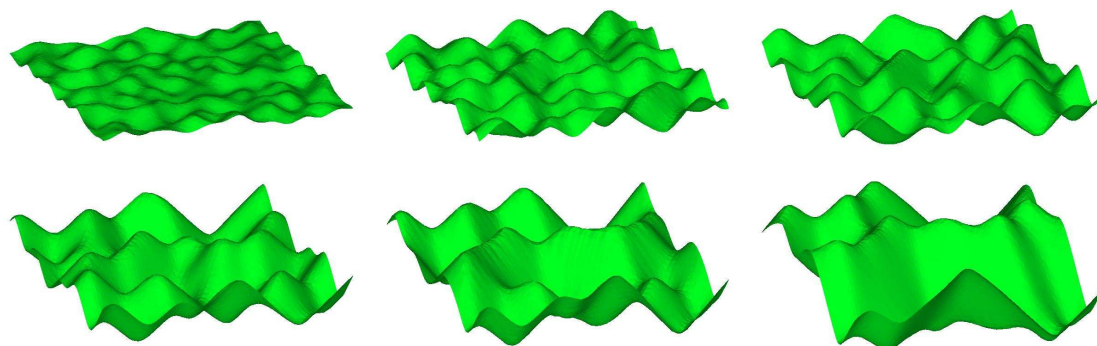


Figure 15: Spinodal decomposition of unstable orientation into pyramidal structure with stable orientations and subsequent coarsening. Simulations are performed by C. Stöcker [13].

We now chose γ such that

$$\gamma(\mathbf{n}) = 1 + \sum_{i=1}^3 n_i^4.$$

Fig. 14 shows the evolution of a sphere towards the Wulff shape under surface diffusion $k=0$, $b=0$ and $\nu=1$. The second example shows the evolution of an initially planar film in an unstable orientation which is randomly perturbed, cf. Fig. 15.

3.4 Comparison of the numerical approaches and limitations

All approaches described above can be used to simulate anisotropic surface evolution laws and the results are comparable. The front tracking method thereby is the most efficient but it has a severe drawback when it comes to topological changes. The computational cost for the phase-field and level-set approaches are comparable. Due to the use of adaptive methods the computational overhead for these methods, resulting from the need to solve the equation in $d+1$ dimensions, is significantly reduced. Using the phase-

field model to simulate the pinch off under surface diffusion leads to results that compare well with the front tracking approach, with the significant difference that the phase-field model can handle the topological change. With the level-set approach we were unable to achieve such a good quantitative agreement. The failure is due to loss of mass in each time step after performing a redistancing step. As the level-set equation does not satisfy a comparison principle our approach can only be interpreted in a local sense. Thus, the level-set function satisfies the PDE only at the zero level-set. This property of locally defined partial differential equations allows us to use special local level-set techniques to solve the level-set equation on a narrow band, cf. e.g. [91]. On the other hand, the level-set function needs to be reinitialized to a signed distance function; and this introduces a systematic loss of mass for closed domains. A smaller enclosed volume, however, leads to a different pinch-off time. The algorithm used to perform the redistancing step follows the approach in Bornemann and Rasch [11] and Stöcker et al. [119]. Higher order schemes, or incorporating additional techniques (e.g., [122,140]) to conserve mass, might be able to overcome the described problem. They are, however, beyond the scope of this paper.

All the approaches allow the use of anisotropies in the free energy density which are not smooth. None of the approaches requires a second derivative of γ . The only requirement is thus convexity as otherwise the evolution equation becomes ill-posed, if no regularization is imposed.

These statements remain true also for the strong anisotropy. All the approaches are in principle able to produce the same results. If in specific applications the topological change is not very important, then the front tracking approach by parametric finite elements can be the method of choice. However, the discretization of the Willmore flow component results in severe problems if no further treatment is applied to ensure grid regularity. As the algorithm moves grid points only in normal direction, they can become irregular. In the case of weakly anisotropic evolution, this was taken care of by applying a tangential movement to regularize the surface mesh following the approach of Bänsch et al. [6]. With the Willmore energy this was found to be no longer sufficient.

A different algorithm for Willmore flow, which accounts for normal and tangential movements was recently introduced by Barrett et al. [8]. However, also in this case it can not be guaranteed that the mesh remains regular. Another possibility is to use a harmonic map from the surface into the sphere, for which a regular grid can be constructed, and then use the inverse mapping to map the regular grid onto the surface. All these approaches add computational complexity and weaken the advantages of the direct front tracking approach. The derivation of the phase-field approach requires some deep understanding of the relation of sharp interface and diffuse interface models with anisotropy. Starting from a physically motivated incorporation of the surface free energy anisotropy into the gradient term of the free energy results in a very complicated set of evolution equations. Incorporating the anisotropy in the way proposed by Torabi et al. [127] leads to a meaningful 6th order evolution law for the phase-field variable. The level-set approach can be derived by simply combining the discretizations for weak

anisotropic evolution and Willmore flow. The problems discussed above, concerning the conservation of mass if reinitialization is required, remain.

4 Applications to crystalline thin films

We now apply the derived geometric evolution laws to various scenarios of the growth of bulk crystals or thin solid films. Accordingly, the applications determine the mass transport mechanisms and the surface evolution may be coupled to bulk effects.

All the described numerical approaches can treat the surface evolution by different mass transport mechanisms with a large variety of anisotropy functions. A non-convex surface free energy γ can be used to model thermal faceting of unstable surfaces. A strong anisotropy in the kinetic coefficient b furthermore allows the simulation of faceting as a result of kinetics, see Uehara and Sekerka [130]. In various situations the evolution, however, might be dominated by the anisotropy in the mobility ν , as seen for example in Krug et al. [70].

The surface evolution not only depends on the specific mass transport mechanisms, the evolution also depends sensitively on the functional form and strength of the various anisotropy functions. A key ingredient for any application is thus the knowledge of the material parameters. The derivation of material-specific forms for the anisotropy functions from atomistic models has only recently become possible. Most of the effort however has been on the estimation of γ . Starting with the work of Asta et al. [3], who measured $\gamma(\mathbf{n})$ for various orientations in molecular dynamic simulations of solid-liquid interfaces, the strength of the anisotropy in γ is today known for several materials. The functional form, however, remains phenomenological. Haxhimali et al. [52] show the importance of the functional form in dendritic evolution. And only recently efforts have been made to derive a material-specific functional form for γ from atomistics, see Majaniemi and Provatas [79]. The functional form and strength of the anisotropy in b , k and ν are less understood. However, similar techniques as used by Asta et al. [3] can also be used to determine the kinetic coefficients, see, e.g., Hoyt et al. [58] and new techniques to measure the strength of ν were recently developed by Trautt et al. [128]. Thus, together with experimental measurements for various orientations, a complete picture is developing which will make material-specific simulations of phase transitions possible.

Realistic simulations of growth phenomena and crystal morphologies require contributions from the bulk phases, which might change the coarsening behavior of faceted surface structures, see [43,48], and which might further lead to mound formation as a result of an Ehrlich-Schwoebel barrier (Bales-Zangwill instability), see [5,34,108,132], or to surface modulations as a result of the Asaro-Tiller-Grinfeld instability, see [2,45,115,116,118]. The former requires a deposition flux and the latter requires an elastically stressed film, e.g. due to an elastic misfit between film and substrate. We discuss these instabilities for different thin film growth regimes.

4.1 Chemical vapor deposition

Chemical vapor deposition (CVD) is a chemical process used to produce high-purity, high-performance solid materials. The process is often used in the semiconductor industry to produce thin films. In a typical CVD process, the substrate is exposed to one or more volatile precursors, which react and/or decompose on the substrate surface to produce the desired deposit. The flux of material on a growing crystal surface is from the diffusion boundary layer whose shape follows the shape of the surface. In this case, the material flux is normal to the surface and significantly changes the surface dynamics.

Within a simplified model we assume the deposition flux to be given

$$F = \mathbf{j} \cdot \mathbf{n}.$$

For more realistic treatments \mathbf{j} needs to be computed by solving appropriate convection-reaction-diffusion equations to account for the mass transport in the growth chamber. If we set for simplicity $\nu = 1$ and $b = 0$ the equation to solve for a strong anisotropic free energy density γ reads

$$\begin{aligned} V &= \Delta_{\Gamma} \mu + F, \\ 0 &= -H_{\gamma} + \alpha^2 \left(\Delta_{\Gamma} H + H \left(\|S\|^2 - \frac{1}{2} H^2 \right) \right) + \mu. \end{aligned}$$

By reformulating the evolution equation in a graph formulation for $h = h(x, y, t)$, using a frame of reference co-moving with the flat interface at speed F , and performing a long-wave approximation, we obtain (see Savina et al. [106])

$$\partial_t h = \frac{1}{2} D |\nabla h|^2 + \Delta \left(\Delta h + \alpha^2 \Delta^2 h - (3h_x^2 + \beta h_y^2) h_{xx} - (3h_y^2 + \beta h_x^2) h_{yy} - 4\beta h_x h_y h_{xy} \right),$$

where D depends on F and β is related to γ . All nonlinear terms related to the curvature regularization are neglected.

The surface dynamics includes an additional, symmetry-breaking convective term that describes the effect of the normal growth. For a one-dimensional surface the equation can be rewritten for the surface slope, $m = h_x$, as

$$\partial_t m = (m_{xx} + m - m^3)_{xxx} + D m m_x, \quad (4.1)$$

which is a higher order convective Cahn-Hilliard equation. Depending on D the dynamic evolution changes dramatically. When D is small, coarsening occurs. As D increases, coarsening is interrupted and spatio-temporal chaos occurs for large D .

Numerical studies in these regimes have been performed by Savina et al. [106]. The long-wave approximation, however, is based on small variations in surface orientation. This introduces a clear limit to the quantitative predictive power of theory in relation to large classes of experimentally observed morphologies, such as facets which meet at high angles of incidence. Detailed coarsening studies within the full geometric setting are shown in Fig. 16. The figure shows the position of kinks (hills, red) and antikinks (valleys, cyan) over time.

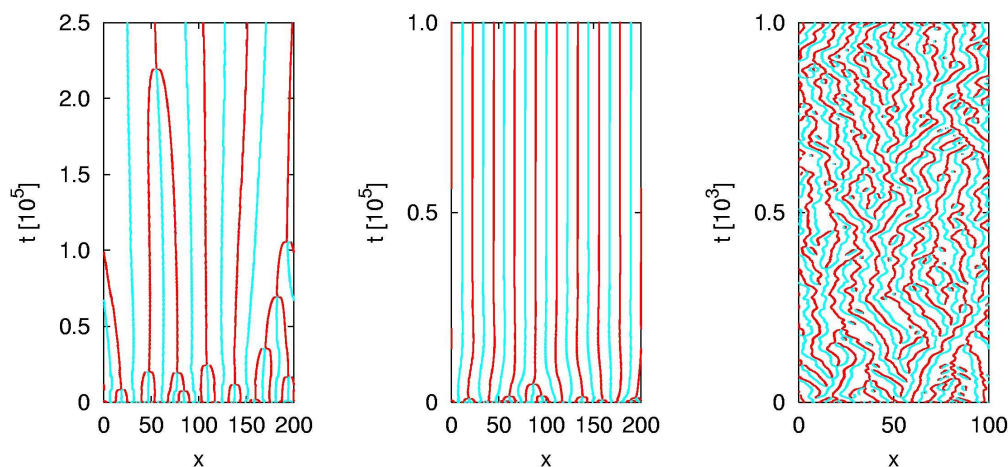


Figure 16: Morphological evolution of hill-valley structures under the influence of a normal deposition flux: (left) $F=0.01$, (middle) $F=0.1$, (right) $F=10$. The simulations are performed by F. Haußer using the front tracking code described in Section 3.1.

4.2 Molecular beam epitaxy

Molecular beam epitaxy (MBE) is a frequently used technique to grow thin solid films on a given substrate [7, 92, 129]. MBE takes place in an ultra vacuum chamber with the deposition of atoms through molecular beams. Chemical bonding leads to flux atoms to be adsorbed on the substrate or the surface of a growing thin film. The microscopic processes of the adsorbed atoms—adatoms—include: diffuse on the surface, evaporate into the vapor usually with small probability, attach to and/or detach from a terrace step, and nucleate a small adatom island. Due to a continuous deposition flux, the growth system is far from equilibrium.

There are two general classes of continuum models of epitaxial growth of thin films. One is the so-called BCF type model which was first developed by Burton-Cabrera-Frank [15]. Such a model consists of diffusion equation for adatom density and moving terrace steps driven by the chemical potential difference from the upper and lower terraces. See e.g., [5, 16, 17, 41, 60, 67, 77, 85, 92–94, 135] and the references therein. Another class of continuum models often consist of partial differential equations of the height profile of the thin films. Often such a height profile of a thin film surface is assumed to have a small slope and various kinds of approximations can then be made. Such models are useful for analytical studies and large scale simulations of the growth and morphologies of thin films, in particular, the coarsening of pyramid structures on the surface of a growing film, see, e.g., [7, 33, 44, 61, 63, 66, 68, 73–75, 81, 86, 92, 102, 103, 112, 132, 133, 139].

Here we consider the second class of continuum models for thin films but try to avoid the small slope assumption. We connect our new model development with the numerical methods for surface evolution described in the previous sections. We shall consider particularly two physical mechanisms. One is the Ehrlich-Schwoebel barrier, which is the

origin of the Bales-Zangwill instability, and the other elastic misfit which is the origin of the Asaro-Tiller-Grinfeld instability.

4.2.1 The Ehrlich-Schwoebel barrier

The Ehrlich-Schwoebel (ES) barrier (see Ehrlich and Hudda [34], Schwobel and Shipsey [108], and Schwobel [107]) is an important kinetic effect that has been well documented experimentally and well studied theoretically. In order to attach to an atomic step, an adatom from an *upper* terrace must overcome an energy barrier—the Ehrlich-Schwoebel barrier—in addition to the diffusion barrier on an atomistically flat terrace. The ES barrier generates an uphill current that destabilizes nominal surfaces (high-symmetry surfaces), but stabilizes vicinal surfaces (stepped surfaces that are in the vicinity of high-symmetry surfaces) with a large slope, preventing step bunching [132]. The ES barrier is the origin of the Bales-Zangwill instability, a diffusional instability of atomic steps [5], cf. also [76]. The ES barrier also affects island nucleation [69]. When the ES barrier is present, the film surface prefers a large slope. The competition between this large-slope preference and the surface relaxation determines the large-scale surface morphology and growth scaling laws [1, 44, 61, 73, 75, 95, 102, 113, 132].

In a basic coarse grained model for epitaxial growth of thin films with the ES barrier, the surface current often takes the form

$$\mathbf{j} = \mathbf{j}_{SD} + \mathbf{j}_{ES},$$

where \mathbf{j}_{SD} describes the current due to the surface diffusion and \mathbf{j}_{ES} the effect of the ES barrier. The surface diffusion current is usually given by

$$\mathbf{j}_{SD} = -\nabla_{\Gamma}(v\Delta_{\Gamma}H),$$

where v is the surface mobility and H is the mean curvature of the growing surface. Anisotropy in the surface diffusion can be incorporated as usual. Various forms of the ES current \mathbf{j}_{ES} have been proposed, cf. Villain [132], Johnson et al. [61], and Stroscio et al. [121]. These forms are given in terms of the surface slope \mathbf{m} , and have the following properties: (i) a linear behavior at small slopes, and (ii) $\mathbf{j}_{ES} = 0$ if $F = 0$.

To connect the description of the ES current with our general theme of geometrical evolution of surfaces with anisotropy, here we propose a general but phenomenological form of the surface current that accounts for the ES effect or other kinetic effects and that includes the anisotropy. We specify \mathbf{j}_{ES} through an effective nonconvex anisotropy function $\beta(\mathbf{n})$, using the Cahn-Hoffmann vector ζ_{β} , with $\zeta_{\beta,i} = \partial_{p_i}\beta$, as

$$\mathbf{j}_{ES} = F\zeta_{\beta}.$$

This leads to $\nabla_{\Gamma} \cdot \mathbf{j}_{ES} = FH_{\beta}$ with $H_{\beta} = \nabla_{\Gamma} \cdot \zeta_{\beta}$ a weighted mean curvature.

Neglecting surface diffusion anisotropy (e.g., $\nu = 1$), the evolution equation now reads

$$V = \Delta_{\Gamma}H - FH_{\beta} + F.$$

Assuming that the surface of a growing film is represented by a height function $h = h(x, y, t)$, and using a co-moving frame $h \rightarrow h - Ft$, then we may obtain a small slope approximation of the above evolution law

$$\partial_t h = -\Delta^2 h + \nabla \cdot W'(\nabla h), \quad (4.2)$$

where $W(\nabla h)$ is defined by

$$\zeta_\beta = \eta W'(\nabla h) + \mathcal{O}(\eta^2),$$

with η an expansion parameter corresponding to the small slope. Appropriate forms for $W'(\nabla h)$ are

$$W'(\nabla h) = -\frac{\nabla h}{1 + |\nabla h|^2}, \quad \text{see [61, 111, 113, 121]},$$

$$W'(\nabla h) = -\frac{\nabla h}{|\nabla h|^2}, \quad \text{see [132]},$$

where the upper function models the effect of a finite ES barrier while the lower function models an infinite ES barrier. These corresponding equations have been studied in detail and various numerical methods have been applied to simulate coarsening (see the references above). Fig. 17 shows contour plots of the height profile h obtained by solving Eq. (4.2) with the upper function $W'(h)$ (finite ES barrier, no slope selection) [75].

For one-dimensional surfaces we can use the approximation $1/(1+h_x^2) \sim 1-h_x^2$ and rewrite the equation in terms of $m = h_x$. We obtain

$$\partial_t m = (-m_{xx} - m + m^3)_{xx}$$

which is a Cahn-Hilliard equation. The double well structure here arises from the kinetics, and in particular, the ES flux. This is in contrast to the example in Eq. (4.1) in Section 4.1, where the same term arose from a strong surface free energy density.

4.2.2 Elastic misfit and the Asaro-Tiller-Grinfeld instability

To study the growth of thin crystalline films, the evolution laws in addition might have to be coupled to an elastic field in the film. The elastic field is incorporated through the bulk free energy density Ψ^+ , which we assume to be equal to the elastic energy density. The evolution equations are

$$V = \nabla \cdot (v \nabla \mu) + F,$$

$$bV = -H_\gamma + \mu - \Psi^+,$$

where (cf., e.g., [62, 71, 72])

$$\Psi^+ = \frac{1}{2} \sum_{i,j,k,l} (E_{ij} - E_{ij}^0) C_{ijkl} (E_{kl} - E_{kl}^0)$$

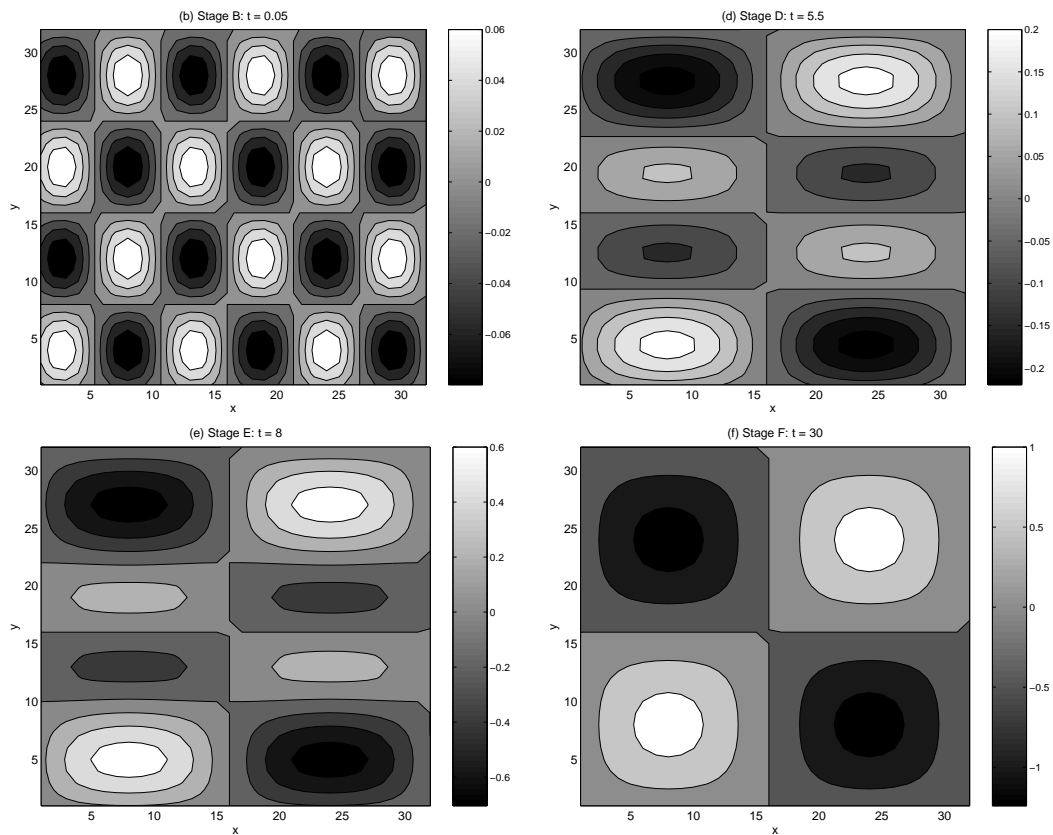


Figure 17: Contour plots of height profiles h , the solution to Eq. (4.2) with $W'(h) = -\frac{\nabla h}{1+|\nabla h|^2}$ (no slope selection) [74].

with C_{ijkl} the stiffness tensor, $E_{ij} = \frac{1}{2}(\frac{\partial u_i}{\partial x_j} + \frac{\partial u_j}{\partial x_i})$ the strain tensor, \mathbf{u} the displacement field and $E_{ij}^0 = E^0 \delta_{ij}$ the misfit strain tensor, with E^0 the coherency strain and δ_{ij} the Kronecker delta. The relation between stress and strain is given by

$$T_{ij} = \sum_k \sum_l C_{ijkl} (E_{kl} - E_{kl}^0).$$

Thus, this system requires the additional solution of an elasticity equation

$$\nabla \cdot \mathbf{T} = 0$$

for the stress field \mathbf{T} in the film. In the simplest setting the boundary condition for the stress field at the interface reads

$$\mathbf{T} \cdot \mathbf{n} = 0.$$

The elastic anisotropy is crucial in the formation of different surface morphologies of thin films.

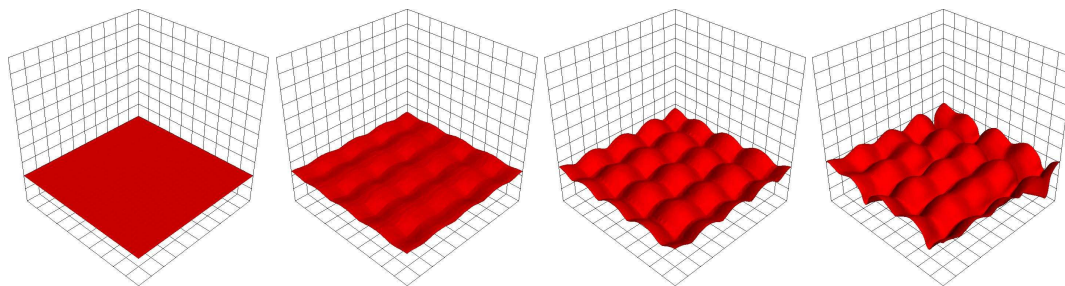


Figure 18: ATG instability of a weakly, anisotropic growing film. Simulations are performed by A. Rätz [97].

The surface evolution now results from the competition between the surface and the elastic energy. The elastic stress is known to lead to the Asaro-Tiller-Grinfeld instability [2, 45, 115, 116, 118]. If the film is relatively thick, the result is essentially equivalent to that of a stressed, semi-infinite solid. In the semi-infinite case, an initial planar surface is unstable and evolves to form a cusp. In the presence of a substrate, the thin films evolve to form islands or nanocrystals. In all simulation results the interface problem, however, is simplified. For example, Fig. 18 shows simulation results within a phase-field setting with a weak anisotropy in γ . A simulation with strong anisotropy, and using the square of the Laplacian of ϕ as the regularization [138], is shown in Fig. 19.

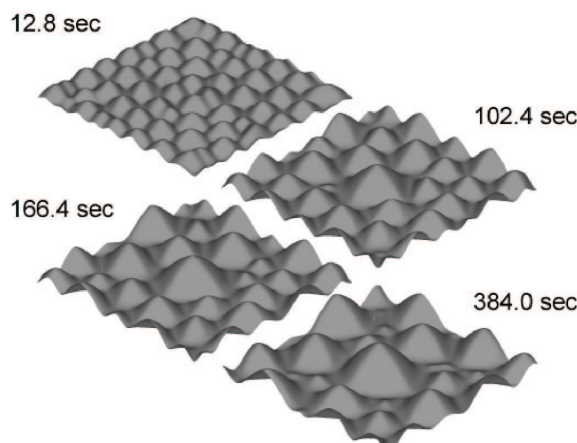


Figure 19: ATG instability of a strongly anisotropic growing film on a patterned substrate with one inclusion. Simulations are performed by S.M. Wise [138].

A detailed description of molecular beam epitaxy thus requires elastic misfit, thermal faceting as a result of strong surface anisotropies, as well as kinetic effects due to an Ehrlich-Schoebel barrier. All three effects lead to different surface instabilities and their competition determines the final surface morphology. Further, a complete picture requires the incorporation of composition gradients due to the presence of different constituents arising from heteroepitaxy, which is beyond the scope of the article.

4.3 Liquid phase epitaxy

Liquid phase epitaxy is a method to grow crystal layers from a melt on solid substrates. The material, that is desired to be deposited on the substrate, is dissolved in the melt of another material. At conditions that are close to the equilibrium between dissolution and deposition, deposition on the substrate is slow and uniform. This allows the production of very thin, uniform and high quality layers. The equilibrium conditions however depend sensitively on the temperature and on the concentration of the dissolved material in the melt. In order to model liquid phase epitaxy with our general approach we need to specify the deposition flux F . Assuming $\mu = \mu^-$, with μ^- the chemical potential in the fluid defined through $\mu^- = \partial_C \Psi^-$ with Ψ^- the bulk free energy of the fluid and C the concentration of the solution in the melt, we may define

$$F = \mathbf{j} \cdot \mathbf{n},$$

with \mathbf{j} defined through the macroscopic equations in the melt. Neglecting flow in the melt and assuming isothermal conditions, we may use Fick's law to get

$$\begin{aligned} \partial_t C &= -\nabla \cdot \mathbf{j}, \\ \mathbf{j} &= -D \nabla C, \end{aligned}$$

with C the concentration of the solution in the melt. Neglecting surface diffusion in the governing equations on the interface gives

$$\begin{aligned} V &= \mathbf{j} \cdot \mathbf{n}, \\ bV &= -H_\gamma + \mu^-. \end{aligned}$$

In the simplest linearized form one may obtain $\mu^- = C^0 - C$, with C^0 an equilibrium concentration. These are the classical interface conditions of mass conservation and the Gibbs-Thomson relation. More detailed studies, however, require strong anisotropies in the surface free energy, the inclusion of kinetic effects associated with the attachment-detachment processes and the coupling of the evolution with the elastic field in the solid.

4.4 Electrodeposition

In electrodeposition, an electric field drives the deposition of a thin film on a substrate from a melt. For example, a negative charge is placed on the substrate. Positively charged metallic ions in the melt are attracted to the substrate which then provides electrons that reduce the ions to metallic form. The method is very cost efficient and is a way to rapidly grow thin films on large area substrates. Despite these advantages, electrodeposition is not widely used in the preparation of functional thin films. One reason is that electrochemically grown films do not achieve the high-quality properties of systems prepared by the previously described methods. This is primarily due to the fact that the properties of the film depend sensitively on the deposition. Here, the deposition is mainly governed

by diffusion, migration and convection, with convection mostly driven by Coulombic forces due to local electric charges and by buoyancy forces due to concentration gradients. A better understanding of the role the deposition plays on the film morphology might thus be a way to help to improve film properties. In order to model electrodeposition with our general approach we need to specify the deposition F and its relation to the ion flux. For example, as in liquid phase epitaxy, we may take

$$F = \mathbf{j} \cdot \mathbf{n}$$

with the flux \mathbf{j} defined through the macroscopic equations in the fluid given by (e.g., [82])

$$\begin{aligned} \partial_t C &= -\nabla \cdot \mathbf{j}, \\ \mathbf{j} &= -\mu C \nabla \phi - D \nabla C + C \mathbf{v}, \\ \Delta \phi &= \frac{e}{\epsilon} z C, \\ \partial_t \mathbf{v} + \mathbf{v} \cdot \nabla \mathbf{v} &= -\frac{1}{\rho_0} \nabla p + \nu \Delta \mathbf{v} + \frac{\mathbf{f}_e}{\rho_0} + \frac{\mathbf{f}_g}{\rho_0}, \\ \nabla \cdot \mathbf{v} &= 0, \end{aligned}$$

with C the concentration, z the number of charges per ion, μ the mobility, D the diffusion coefficient of the ion. Further, ϕ is the electrostatic potential, e the electric charge, ϵ the permeability of the medium, \mathbf{v} the fluid velocity, p the pressure, ν the kinematic viscosity and ρ_0 a reference fluid density. The forcing functions due to Coulombic and buoyancy forces are given by

$$\mathbf{f}_e = e \mathbf{E} z C, \quad \mathbf{f}_g = \rho \mathbf{g},$$

where \mathbf{E} is the electric field, \mathbf{g} the gravitational acceleration and ρ the density defined through the Boussinesq approximation

$$\rho = \rho_0 (1 + \alpha \Delta C).$$

Again neglecting surface diffusion in the governing equations on the interface and assuming $\mu = \mu^-$ give the same equations on the interface as in the case of liquid phase epitaxy, namely

$$\begin{aligned} V &= \mathbf{j} \cdot \mathbf{n}, \\ bV &= -H_\gamma + \mu^-. \end{aligned}$$

As in the previously discussed cases, quantitative studies of the growth processes also require the incorporation of additional effects such as surface energy anisotropy, kinetics, elasticity, etc.

5 Conclusions

We have presented a brief survey of the basic theory of geometrical evolution laws, finite-element based numerical methods for the simulation of interfacial motion, and applications of the geometrical evolution models coupled with other physical effects to thin film growth and morphologies.

The interface evolution laws we review here are variants of the motion by mean curvature, the motion by mean curvature with a constrained volume and the motion by the Laplacian of mean curvature. We have placed all these laws in a single, unifying framework which corresponds to a descent dynamics of an effective surface free energy. We pay a special attention to strong surface energy anisotropy.

We have reviewed the recent development of numerical methods and techniques for various kinds interface motions. This includes the front tracking method, and the phase-field and level-set methods. The most noticeable progress achieved has been the development of the numerical methods for high order problems and for coupled systems. All of these methods we have reviewed are based on the finite element approach. One reason for using a finite element method is that the geometrical evolution laws are variational in nature, and thus this approach may take advantage of weak formulation. Another potential advantage of the finite element method for surface motion is that high accuracy can be achieved when a body-fitted, conforming, finite element mesh is constructed. We believe, however, that other methods of discretization, and in particular adaptive finite difference methods, also have their advantages. There is a large literature on finite difference methods for front tracking, phase-field and level-set computations of interface dynamics; this is beyond the scope of this review.

Finally we have reviewed some of the applications of geometrically based interface models to study the growth and surface morphologies of thin crystalline films. We have presented extensive numerical results that demonstrate that the existing numerical methods can capture qualitatively the physical properties of thin films.

While much progress has been made in the development of models, algorithms and applications, there is much more work to be done. For example, rigorous mathematical and numerical analyses are needed to guide the design of accurate and efficient numerical methods. In particular, the issue of high-order regularization, needed for strong surface energy anisotropy, requires further investigation. Also, multiscale models of interface dynamics in materials are needed that can link microscopic processes to larger scales in order to provide accurate parameters and constitutive laws for macroscopic numerical computations.

Acknowledgments

The authors would like to thank Frank Haußer, Pedro Morin, Christina Stöcker, Solmaz Torabi and Steven Wise for providing us with their simulation results and Martin Burger,

Joachim Krug, Steven Wise and Stephen Watson for fruitful discussions. The work of B. Li was supported by the US National Science Foundation (NSF) through grants DMS-0451466 and DMS-0811259, by the US Department of Energy through grant DE-FG02-05ER25707, and by the Center for Theoretical Biological Physics through the NSF grants PHY-0216576 and PHY-0822283. J. Lowengrub gratefully acknowledges support from the US National Science Foundation Divisions of Mathematical Sciences (DMS) and Materials Research (DMR). The work of A. Voigt and A. Rätz was supported by the 6th Framework program of EU STRP 016447 and German Science Foundation within the Collaborative Research Program SFB 609. We further acknowledge the computing support provided by the ZIH (Zentrum für Informationsdienste und Hochleistungsrechnen) at TU Dresden.

References

- [1] J. G. Amar and F. Family. Effects of crystalline microstructure on epitaxial growth. *Phys. Rev. B*, 54(20):14742–14753, 1996.
- [2] R. Asaro and W.A. Tiller. Interface morphology development during stress corrosion cracking: Part I. via diffusion. *Metall. Trans.*, 2:1789–1796, 1972.
- [3] M. Asta, J.J. Hoyt, and A. Karma. Method for computing the anisotropy of the solid-liquid interfacial free energy. *Phys. Rev. Lett.*, 86:5530, 2001.
- [4] R. Backofen, A. Rätz, and A. Voigt. Equilibrium shapes of nanocrystals - computed using a phase field crystal model. *J. Crystal growth*, in review.
- [5] G.S. Bales and A. Zangwill. Morphological instability of a terrace edge during step flow growth. *Phys. Rev. B*, 41:5500, 1990.
- [6] E. Bänsch, P. Morin, and R.H. Nochetto. A finite element method for surface diffusion: the parametric case. *J. Comput. Phys.*, 203:321–343, 2005.
- [7] A.-L. Barabási and H. E. Stanley. *Fractal Concepts in Surface Growth*. Cambridge University Press, Cambridge, 1995.
- [8] J. Barrett, H. Garcke, and R. Nuernbeg. On the parametric finite element approximation of evolving hypersurfaces in \mathbb{R}^3 . *J. Comput. Phys.*, 227:4281–4307, 2008.
- [9] T. Biben, K. Kassner, and C. Misbah. Phase-field approach to three-dimensional vesicle dynamics. *Phys. Rev. E*, 72:049121, 2005.
- [10] T. Biben and C. Misbah. Tumbling of vesicles under shear flow with an advected-field approach. *Phys. Rev. E*, 67:031908, 2003.
- [11] F. Bornemann and C. Rasch. Finite-Element discretization of static Hamilton-Jacobi equations based on a local variational principle. *Comput. Vis. Sci.*, 2006.
- [12] C. R. Brundle, C.A. Evans, Jr., and S. Wilson. *Encyclopedia of Materials Characterization*. Butterworth-Heinemann, 1992.
- [13] M. Burger, F. Haußer, C. Stöcker, and A. Voigt. A level set approach to anisotropic flow with curvature regularization. *J. Comput. Phys.*, 225:183–205, 2007.
- [14] M. Burger, C. Stöcker, and A. Voigt. Finite element based level set method for higher order flows. *J. Sci. Comput.*, in press.
- [15] W.K. Burton, N. Cabrera, and F.C. Frank. The growth of crystals and the equilibrium of their surfaces. *Phil. Trans. Roy. Soc. London A*, 243(866):299–358, 1951.
- [16] R. E. Caflisch, W. E. M. F. Gyure, B. Merriman, and C. Ratsch. Kinetic model for a step edge in epitaxial growth. *Phys. Rev. E*, 59(6):6879–6887, 1999.

- [17] R. E. Caflisch and B. Li. Analysis of island dynamics for epitaxial growth of thin films. *Multiscale Modeling and Simulation*, 1(1):150–171, 2003.
- [18] R.E. Caflisch. Growth, structure and pattern formation for thin films. *J. Sci. Comput.*, 37:3–17, 2008.
- [19] J.W. Cahn, C.M. Elliott, and A. Novick-Cohen. The Cahn-Hilliard equation with a concentration dependent mobility: motion by minus the Laplacian of the mean curvature. *Euro. J. Appl. Math.*, 7:287–301, 1996.
- [20] J.W. Cahn and D.W. Hoffman. A vector thermodynamics for anisotropic surfaces ii. curved and faceted surfaces. *Acta Metall. Mater.*, 22:1205–1214, 1974.
- [21] J.W. Cahn and J.E. Taylor. Linking anisotropic sharp and diffuse surface motion laws via gradient flows. *J. Stat. Phys.*, 77:404–423, 1994.
- [22] J.W. Cahn and J.E. Taylor. Surface motion by surface-diffusion. *Acta Metall.*, 42:1045–1063, 1994.
- [23] P. Cermelli and M.E. Jabbour. Multispecies epitaxial growth on vicinal surfaces with chemical reactions and diffusion. *Phil. Trans. Roy. Soc. London A*, 461:3483–3504, 2005.
- [24] A. Chatterjee and D.G. Vlachos. An overview of spatial microscopic and accelerated kinetic monte carlo methods. *J. Computer-Aided Mater. Des.*, 14:253–308, 2007.
- [25] U. Clarenz, F. Haußer, M. Rumpf, A. Voigt, and U. Weikard. On level set formulations for anisotropic fourth order geometric evolution problems. In A. Voigt, editor, *Multiscale modeling in epitaxial growth*, pages 227–237. Birkhäuser, 2005.
- [26] J.-M. Debievre, A. Karma, F. Celestini, and R. Guerin. Phase-field approach for faceted solidification. *Phys. Rev. E*, 68:041604, 2003.
- [27] K. Deckenick, G. Dziuk, and C.M. Elliott. Computation of geometric partial differential equations. *Acta Numer.*, pages 1–94, 2005.
- [28] K. Deckenick, G. Dziuk, and C.M. Elliott. Fully discrete finite element approximation for anisotropic surface diffusion of graphs. *SIAM J. Numer. Anal.*, 43:1112–1138, 2005.
- [29] A. DiCarlo, M.E. Gurtin, and P. Podio-Guidugli. A regularized equation for anisotropic motion-by-curvature. *SIAM J. Appl. Math.*, 52(4):1111–1119, 1992.
- [30] M. Droske and M. Rumpf. A level set formulation for Willmore flow. *Interf. Free Bound.*, 6:361–378, 2004.
- [31] Q. Du, C. Liu, and X. Wang. A phase field formulation of the Willmore problem. *Nonlin.*, 18:1249–1267, 2005.
- [32] G. Dziuk. An algorithm for evolving surfaces. *Numer. Math.*, 58:603–611, 1991.
- [33] S. F. Edwards and D. R. Wilkinson. The surface statistics of a granular aggregate. *Proc. Roy. Soc. A*, 381:17–31, 1982.
- [34] G. Ehrlich and E.J. Hudda. Atomic view of surface diffusion: tungsten on tungsten. *J. Chem. Phys.*, 44:1039–1099, 1966.
- [35] C.M. Elliott and H. Garcke. Existence results for diffuse surface motion laws. *Adv. Math. Sci. Appl.*, 7:465–488, 1997.
- [36] H. Emmerich. Advances of and by phase-field modeling in condensed-matter physics. *Adv. Phys.*, 57:1–87, 2008.
- [37] J.W. Evans, P.A. Thiel, and M.C. Bartelt. Morphological evolution during epitaxial thin film growth: Formation of 2d islands and 3d mounds. *Surf. Sci. Reports*, 61:1–129, 2006.
- [38] L.C. Evans, H.M. Soner, and P.E. Souganidis. Phase-transitions and generalized motion by mean-curvature. *Comm. Pure. Appl. Math.*, 45:1097–1123, 1992.
- [39] X. Feng and A. Prohl. Numerical analysis of the allen-cahn equation and approximation for mean curvature flow. *Numer. Math.*, 94:33–65, 2003.

- [40] E. Fried and M. Gurtin. A unified treatment of evolving interfaces accounting for small deformations and atomic transport with emphasis on grain-boundary and epitaxy. *Adv. Appl. Mech.*, 40:1–178, 2004.
- [41] R. Ghez and S. S. Iyer. The kinetics of fast steps on crystal surfaces and its application to the molecular beam epitaxy of silicon. *IBM J. Res. Develop.*, 32:804–818, 1988.
- [42] E. De Giorgi. Some remarks on Γ -convergence and least square methods. In G. Del Masso and G.F. Dell’Antonio, editors, *Progress in Nonlinear Differential Equations and their Applications*, volume 5, pages 135–142. Birkhäuser, 1991.
- [43] A.A. Golovin, A.A. Nepomnyashchy, S.H. Davis, and M.A. Zaks. Convective Cahn-Hilliard models: From coarsening to roughening. *Phys. Rev. Lett.*, 86:1550–1553, 2001.
- [44] L. Golubović. Interfacial coarsening in epitaxial growth models without slope selection. *Phys. Rev. Lett.*, 78(1):90–93, 1997.
- [45] M.A. Grinfeld. Instability of the separation boundary between a non-hydrostatically stressed elastic body and a melt. *Sov. Phys. Dokl.*, 31:831–834, 1986.
- [46] M.E. Gurtin and M.E. Jabbour. Interface evolution in three dimensions with curvature-dependent energy and surface diffusion: Interface-controlled evolution, phase transitions, epitaxial growth of elastic films. *Arch. Rat. Mech. Anal.*, 163:171–208, 2002.
- [47] F. Hauser and A. Voigt. A discrete scheme for regularized anisotropic surface diffusion, a 6th order geometric evolution equation. *Interf. & Free Bound.*, 7:353–370, 2005.
- [48] F. Hauser and A. Voigt. Facet formation and coarsening modeled by a geometric evolution law for epitaxial growth. *J. Crystal Growth*, 275:e47–e51, 2005.
- [49] F. Hauser and A. Voigt. A numerical scheme for regularized anisotropic curve shortening flow. *Appl. Math. Lett.*, 19:691–698, 2006.
- [50] F. Hauser and A. Voigt. A discrete scheme for parametric anisotropic surface diffusion. *J. Sci. Comput.*, 30:223–235, 2007.
- [51] F. Hauser and A. Voigt. A geometric ginzburg-landau theory for faceted crystals in 1d: from coarsening to chaos through a driving force. *Phys. Rev. E*, in review.
- [52] T. Haxhimali, A. Karma, F. Gonzales, and M. Rappaz. Orientation selection in dendritic evolution. *nature materials*, 5:660–604, 2006.
- [53] C. Herring. Some theorems on the free energies of crystal surfaces. *Phys. Rev.*, 82:87–93, 1951.
- [54] C. Herring. Surface tension as a motivation for sintering. In W. E. Kingston, editor, *The Physics of Powder Metallurgy*, pages 143–179. McGraw-Hill, 1951.
- [55] C. Herring. The use of classical macroscopic concepts in surface energy problems. In R. Gomer and C. S. Smith, editors, *Structure and Properties of Solid Surfaces*, pages 2–72. Univ. of Chicago Press, 1953.
- [56] D. W. Hoffman and J. W. Cahn. A vector thermodynamics for anisotropic surfaces. I. *Surf. Sci.*, 31:368–388, 1972.
- [57] J.M. Howe. *Interfaces in Materials*. Wiley-Interscience, 1997.
- [58] J.J. Hoyt, M. Asta, and A. Karma. Atomistic simulation methods for computing the kinetic coefficient in solid-liquid systems. *Interface Sci.*, 10:181–189, 2002.
- [59] D. Jamet and C. Misbah. Toward a thermodynamically consistent picture of the phase-field model of vesicles: Curvature energy. *Phys. Rev. E*, 78:031902, 2008.
- [60] H.-C. Jeong and E. D. Williams. Steps on surfaces: experiment and theory. *Surface Sci. Reports*, 34:171–294, 1999.
- [61] M.D. Johnson, C. Orme, A.W. Hunt, D. Graff, J. Sudijono, L.M. Sander, and B.G. Orr. Stable and unstable growth in molecular beam epitaxy. *Phys. Rev. Lett.*, 64, 1994.

- [62] W.C. Johnson and W.I.D Alexander. Interfacial conditions for thermomechanical equilibrium in two-phase crystal. *J. Appl. Phys.*, 59:2735, 1986.
- [63] M. Kardar, G. Parisi, and Y. C. Zhang. Dynamic scaling of growing interfaces. *Phys. Rev. Lett.*, 56:889–892, 1986.
- [64] D. Kessler, R.H. Nochetto, and A. Schmidt. Numerical analysis of the allen-cahn equation and approximation for mean curvature flow. *Math. Model. Numer. Anal.*, 38:129–142, 2004.
- [65] R. Kobayashi. Modeling and numerical simulations of dendritic crystal growth. *Physica D*, 63:410–423, 1993.
- [66] R. V. Kohn and X. Yan. Upper bounds on the coarsening rate for an epitaxial growth model. *Commun. Pure Appl. Math.*, 56(11):1549–1564, 2003.
- [67] J. Krug. Four lectures on the physics of crystal growth. *Physica A*, 313:47–82, 2002.
- [68] J. Krug, M. Plischke, and M. Siegert. Surface diffusion currents and the universality classes of growth. *Phys. Rev. Lett.*, 70(21):3271–3274, 1993.
- [69] J. Krug, P. Politi, and T. Michely. Island nucleation in the presence of step-edge barriers: Theory and applications. *Phys. Rev. B*, 61(20):14037–14046, 2000.
- [70] P. Kuhn, J. Krug, F. Hausßer, and A. Voigt. Complex shape evolution in electromigration driven single layer islands. *Phys. Rev. Lett.*, 2005.
- [71] F.C. Larche and J.W. Cahn. Thermodynamic equilibrium of multiphase solids under stress. *Acta Metall.*, 26:1579, 1978.
- [72] P.H. Leo and R.F. Sekerka. The effect of surface stress on crystal melt and crystal-crystal equilibrium. *Acta Metall.*, 37:3139, 1989.
- [73] B. Li. High-order surface relaxation vs. the Ehrlich-Schwoebel effect. *Nonlinearity*, 19:2581–2603, 2006.
- [74] B. Li and J.-G. Liu. Thin film epitaxy with or without slope selection. *European J. Appl. Math.*, 14(6):713–743, 2003.
- [75] B. Li and J.G. Liu. Epitaxial growth without slope selection: energetics, coarsening, and dynamic scaling. *J. Nonlin. Sci.*, 14:429–451, 2004.
- [76] B. Li, A. Rätz, and A. Voigt. Stability of a circular epitaxial island. *Physica D*, 198:231–247, 2004.
- [77] F. Liu and H. Metiu. Stability and kinetics of step motion on crystal surfaces. *Phys. Rev. E*, 49(4):2601–2616, 1997.
- [78] P. Loreti and R. March. Propagation of fronts in a nonlinear fourth order equation. *Euro. J. Appl. Math.*, 11:203–213, 2000.
- [79] S. Majaniemi and N. Provatas. personal communication. 2007.
- [80] M.A. Makeev. Self-organized quantum dot superstructures for nanoelectronic and optoelectronic applications. *J. Nanoelectronics and Optoelectronics*, 1:176–193, 2006.
- [81] D. Margetis and R. Kohn. Continuum relaxation of interacting steps on crystal surfaces in 2+1 dimensions. *Multiscale Model. Sim.*, 5:729–758, 2006.
- [82] G. Marshall, P. Mocoskos, H.L. Swinney, and J.M. Huth. Buoyancy and electrically driven convection models in thin-layer electrodeposition. *Phys. Rev. E*, 59:2157–2167, 1999.
- [83] G.B. McFadden. Phase-field models for solidification. *Contem. Math.*, 306:107–145, 2002.
- [84] G.B. McFadden, A.A. Wheeler, R.J. Braun, S.R. Coriell, and R.F. Sekerka. Phase-field models for anisotropic interfaces. *Phys. Rev. E*, 48:2016–2024, 1993.
- [85] T. Michely and J. Krug. Islands, mounds, and atoms: patterns and processes in crystal growth far from equilibrium. Springer, 2004.
- [86] D. Moldovan and L. Golubović. Interfacial coarsening dynamics in epitaxial growth with slope selection. *Phys. Rev. E*, 61(6):6190–6214, 2000.

- [87] C. Müller-Gugenberger, R. Spatschek, and K. Kassner. Comparison of phase-field models for surface diffusion. *Phys. Rev. E*, in press, 2008.
- [88] W.W. Mullins. 2-dimensional motion of idealized grain boundaries. *J. Appl. Phys.*, 27:900–904, 1956.
- [89] W.W. Mullins. Theory of thermal grooving. *J. Appl. Phys.*, 28:333–339, 1957.
- [90] S. Osher and J. Sethian. Front propagation with curvature-dependent speed - algorithms based on Hamilton-Jacobi formulations. *J. Comput. Phys.*, 79:12–49, 1988.
- [91] D. Peng, B. Merriman, S. Osher, H. Zhao, and M. Kang. A PDE based fast local level set method. *J. Comput. Phys.*, 155:410–438, 1999.
- [92] A. Pimpinelli and J. Villain. *Physics of Crystal Growth*. Cambridge University Press, 1998.
- [93] A. Pimpinelli, J. Villain, D. E. Wolf, J. J. Métois, J. C. Heyraud, I. Elkinani, and G. Uimin. Equilibrium step dynamics on vicinal surfaces. *Surface Sci.*, 295:143, 1993.
- [94] P. Politi, G. Grenet, A. Marty, A. Ponchet, and J. Villain. Instabilities in crystal growth by atomic or molecular beams. *Phys. Reports*, 324:271–404, 2000.
- [95] P. Politi and A. Torcini. Coarsening in surface growth models without slope selection. *J. Phys. A: Math. Gen.*, 33:L77–L82, 2000.
- [96] A. Rätz. PhD thesis, Universität Bonn, 2007.
- [97] A. Rätz, A. Ribalta, and A. Voigt. Surface evolution of elastically stressed film under deposition by a diffuse interface model. *J. Comput. Phys.*, 214:187–208, 2006.
- [98] A. Rätz and A. Voigt. Higher order regularization of anisotropic geometric evolution equations in three dimensions. *J. Theor. Comput. Nanosci.*, 3:560–564, 2006.
- [99] N. Reinecke and E. Taglauer. The kinetics of oxygen-induced faceting of Cu(115) and Cu(119) surfaces. *Surf. Sci.*, 454:94–100, 2000.
- [100] M. Röger. personal communication, 2006.
- [101] M. Röger and R. Schätzle. On a modified conjecture of De Giorgi. *Mathematische Zeitschrift*, 254:675–714, 2006.
- [102] M. Rost and J. Krug. Coarsening of surface structures in unstable epitaxial growth. *Phys. Rev. E*, 55(4):3952–3957, 1997.
- [103] M. Rost, P. Šmilauer, and J. Krug. Unstable epitaxy on vicinal surfaces. *Surface Sci.*, 369:393–402, 1996.
- [104] J. Rubinstein and P. Sternberg. Nonlocal reaction diffusion-equations and nucleation. *IMA J. Appl. Math.*, 48:249–254, 1992.
- [105] R. Rusu. An algorithm for elastic flows of surfaces. *Interf. Free Bound.*, 7:229–239, 2005.
- [106] T.V. Savina, A.A. Golovin, S.H. Davis, A.A. Nepomnyashchy, and P.W. Voorhees. Faceting of growing crystal surfaces by surface diffusion. *Phys. Rev. E*, 67:021606, 2003.
- [107] R. L. Schwoebel. Step motion on crystal surfaces II. *J. Appl. Phys.*, 40:614–618, 1969.
- [108] R.L. Schwoebel and E.J. Shipsey. Step motion on crystal surfaces. *J. Appl. Phys.*, 37:3682–3686, 1966.
- [109] R. Sekerka. Analytical criteria for missing orientations on three-dimensional equilibrium shapes. *J. Cryst. Growth*, pages 77–82, 2005.
- [110] M. Siegel, M.J. Miksis, and P.W. Voorhees. Evolution of material voids for highly anisotropic surface energy. *J. Mech. Phys. Sol.*, 52:1319–1353, 2004.
- [111] M. Siegert. Ordering dynamics of surfaces in molecular beam epitaxy. *Physica A*, 239:420–427, 1997.
- [112] M. Siegert. Coarsening dynamics in crystalline thin films. *Phys. Rev. Lett.*, 81(25):5481–5484, 1998.
- [113] M. Siegert and M. Plischke. Slope selection and coarsening in molecular beam epitaxy.

- Phys. Rev. Lett., 73:1517, 1994.
- [114] P. Smereka. Semi-implicit level set methods for curvature and surface diffusion motion. *J. Sci. Comput.*, 19:439–456, 2003.
 - [115] B. J. Spencer, P. W. Voorhees, and S. H. Davis. Morphological instability in epitaxially-strained dislocation-free solid films: linear stability theory. *J. Appl. Phys.*, 73:4955–4970, 1993.
 - [116] B. J. Spencer, P. W. Voorhees, and S. H. Davis. Morphological instability in epitaxially-strained dislocation-free solid films: nonlinear evolution. *Phys. Rev. B*, 47:9760–9777, 1993.
 - [117] B.J. Spencer. Asymptotic solutions for the equilibrium crystal shape with small corner energy regularization. *Phys. Rev. E*, 69:011603, 2004.
 - [118] D. J. Srolovitz. On the stability of surfaces of stressed solids. *Acta metall.*, 37(2):621–625, 1989.
 - [119] C. Stöcker, S. Vey, and A. Voigt. AMDiS- adaptive multidimensional simulations: composite finite elements and signed distance functions. *WSEAC Trans. Circ. Syst.*, 4:111–116, 2005.
 - [120] C. Stöcker and A. Voigt. The effect of kinetics in the surface evolution of thin crystalline films. *J. Cryst. Growth*, 303:90–94, 2007.
 - [121] J.A. Strosio, D.T. Pierce, M.D. Stiles, A. Zangwill, and L.M. Sander. Coarsening of unstable surface features during Fe(001) homoepitaxy. *Phys. Rev. Lett.*, 75:4246, 1995.
 - [122] M. Sussman, E. Fatemi, P. Smereka, and S. Osher. An improved level-set method for incompressible two-phase flows. *Comput. Fluids*, 277:663–680, 1998.
 - [123] A.P. Sutton and R.W. Balluffi. *Interfaces in Crystalline Materials*. Oxford University Press, 1997.
 - [124] A. Szczepkowicz, A. Ciszewski, R. Bryl, C. Oleksy, C.-H. Nien, Q. Wu, and T.E. Madey. A comparison of adsorbate-induced faceting on flat and curved crystal surfaces. *Surf. Sci.*, 599:55–68, 2005.
 - [125] J.E. Taylor. Mean curvature and weighted mean curvature. *Acta Metall. Mater.*, 40:1475–1485, 1992.
 - [126] T. Tiedje and A. Ballestad. Atomistic basis for continuum growth equation: Description of morphological evolution of GaAs during molecular beam epitaxy. *Thin Solid Films*, 516:3705–3728, 2008.
 - [127] S. Torabi, S. Li, A. Rätz, S. Wise, A. Voigt, and J. Lowengrub. Diffuse interface modeling of strongly anisotropic systems. *Proc. Roy. Soc. A*, in press.
 - [128] Z.T. Trautt, M. Upmanyu, and A. Karma. Interface mobility from interface random walk. *Science*, 314:632–637, 2006.
 - [129] J. Y. Tsao. *Materials Fundamentals of Molecular Beam Epitaxy*. Academic Press, 1993.
 - [130] T. Uehara and R.F. Sekerka. Phase field simulations of faceted growth for strong anisotropy of kinetic coefficient. *J. Cryst. Growth*, 254:252–261, 2003.
 - [131] S. Vey and A. Voigt. AMDiS: adaptive multidimensional simulations. *Comput. Vis. Sci.*, 10:57–67, 2007.
 - [132] J. Villain. Continuum models of crystal growth from atomic beams with and without desorption. *J. de Phys.*, 1:19–42, 1991.
 - [133] D. D. Vvedensky, A. Zangwill, C. N. Luse, and M. R. Wilby. Stochastic equations of motion for epitaxial growth. *Phys. Rev. E*, 48:852–862, 1993.
 - [134] A.A. Wheeler. Phase-field theory of edges in an anisotropic crystal. *Proc. Royal Soc. A*, 462:3363–3384, 2006.
 - [135] R. S. Williams and W. M. Tong. Kinetics of surface growth: Phenomenology, scaling, and

- mechanisms of smoothing and roughening. *Ann. Rev. Phys. Chem.*, 45:401–438, 1994.
- [136] T.J. Willmore. *Riemannian geometry*. Oxford University Press, 1993.
- [137] S. Wise, J.-S. Kim, and J.S. Lowengrub. Solving the regularized, strongly anisotropic Cahn-Hilliard equation by an adaptive nonlinear multigrid method. *J. Comp. Phys.*, 226:414–446, 2007.
- [138] S. Wise, J. Lowengrub, J.S. Kim, K. Thornton, P.W. Voorhees, and W.C. Johnson. Quantum dot formation on a strain-patterned epitaxial thin film. *Appl. Phys. Lett.*, 87:133102, 2005.
- [139] D. E. Wolf and J. Villain. Growth with surface diffusion. *Europhys. Lett.*, 13:389–394, 1990.
- [140] J.-J. Xu, Z. Li, J.S. Lowengrub, and H. Zhao. A level-set method for interfacial flows with surfactant. *J. Comput. Phys.*, 212:590–616, 2006.